INVESTIGATIONS OF ELECTRONIC STRUCTURE OF BARE AND PASSIVATED NANOCRYSTALLINE SILICON CLUSTERS AND THEIR TRANSPORT PROPERTIES

By

SOLOMUN TEKLAHYMANOT TESFAY

A THESIS SUBMITTED IN PARTIAL FULFILMENT OF THE REQUIREMENT FOR THE DEGREE OF MASTER OF SCIENCE IN MATERIALS SCIENCE AT ADDIS ABABA UNIVERSITY SCHOOL OF GRADUATE STUDIES

ADDIS ABABA, ETHIOPIA

ADDIS ABABA UNIVERSITY
GRADUATE STUDIES
INVESTIGATIONS OF ELECTRONIC STRUCTURE OF BARE AND PASSIVATED NANOCRYSTALLINE SILICON CLUSTERS AND THEIR TRANSPORT PROPERTIES

By: Solomun Teklahymanot

Materials Science Program
College of Natural Science

Approved by the Examining Board

Prof. Javed Mazher
(Advisor)

Dr. Gebremedhn G/Yesus
(Examiner)

Dr. B. Tilak
(Examiner)

Prof. Teketel Yohannes
(Chairperson)

Acknowledgement

It is difficult to overstate my gratitude to my supervisor Professor Javed Mazher. With his enthusiasm, his inspiration, explanations of things clearly and simply, he helped me. Throughout my thesis-writing period, he provided encouragement, sound advice, good teaching, good company, and lots of good ideas.

I am indebted to my many student colleagues for providing a stimulating and fun environment in which to learn and grow. I am especially grateful to Professor Teketel Yohannes, for his giving me constructive advice.

I wish to thank my entire extended family for providing a loving environment for me. My brothers, my sister, were particularly supportive.

Lastly, and most importantly, I wish to thank my parents, they bore me, raised me, supported me, taught me, and loved me. To them I dedicate this thesis.

Table of content

List of table

List of figures

Abstract

Silicon low dimensional structures are found to be extremely stable in comparison to bulk silicon along with variety of interesting electronic properties. They are established as potential candidates for various promising applications in advanced nano-electronics devices especially in a nano-switch to be specific. Here we are presenting our most recent and most detailed results for electronic and transport properties of ground-state structures of Sin, SinH and SinO clusters using DFT- LDA-NEGF simulations. From our present set of studies, a high degree of structural stability is observed in very small Si_n nanoclusters of various sizes; n = 4, 6, 7 and 8. Amongst several diverse and stable clusters, the Si6 is found to possess a maximum stability. The energy gaps in between LUMO-HOMO of Si clusters are also found to be decreasing with the "n" in accordance with general principles of a quantum confinement with an exception of the Si6 cluster. Density of states spectra (DOS), transmission spectrum (TS) and current-voltage (I-V) calculations are also preformed. Various TS spectra results are mostly discussed in contest to charge transfer phenomena, states injection in between various components of the nanodevices and their ensuing effects on the nanoswitching. We have also ascertained increased cluster stability with the passivation and the presence of a significant contributing states at fermi energies in nano devices that are made up of these clusters. A novel phenomenon of a negative differential resistance becomes pragmatic in I-V curves of these samples and it is discussed in relation to the Q-confinement induced singularities among the concerned nanostructures. I-V characteristics curve of a device ZGNR/Si8H/ZGNR shows strong nonlinearity as a result it can be fruitfully deployed for the nano-switch. Various lurid prospects of nano-swtcing using Si_n nanoclusters are also conferred in the present work.

Chapter one

1. Introduction

Silicon low-dimensional structures possess a variety of interesting electronic properties. A lot of recent research has already been focused on decreasing size of the crystal and related quantum confinement effects which enlarge materials band-gap energy, and which can possibly lead to a change of its character from indirect to direct gap material, which further enhances luminescence efficiencies of such nanomaterials. Both effects have already detected by optical methods due to an increased efficiency of the emission and its gradual shift to higher energies upon the size reduction [1]. Unfortunately, low-dimensional structures are also characterized by a large surface-to-volume ratio. Surface-related effects obscure an observation and a conclusive identification of quantum-confinement-related effects [2]. However, it has been theoretically known for more than a decade that very small Si_n nanoclusters comprise of only few atoms are highly stable and possess the magic atomic number configurations after a pioneering piece of work by Pan et. al [3]. Such stability of silicon clusters is mainly accredited from a capability of Si self-assembly by virtue of which the very small Si nanoclusters are able to generate unique geometrical structures without any dangling bonds in their structural models, as proposed by the Pan et. al. Hence in analogies of a atomic stability associated with magic numbers, which are found in shell models of both atomic and nuclear structures and implies a series of numbers that indicate structural stable, the authors have rightly termed the numbers 'n' as the magic numbers for stable Si small clusters. Such Si_n clusters are found to be exceptionally stable in respect to both the geometry as well as electronic band structure [4]. Until date, the Silicon researchers have discovered a range of magic numbers, which are validated experimentally and theoretically; values of 'n' = 4, 6, 7, 8, 9, 13, 14 and 23 are found to be most stable [5]. Because of quantum confinement related effects, the silicon low-dimensional nanoclusters are potential candidates for various promising applications in advanced optoelectronic and electronic devices, apart from this various fundamental physical properties of the silicon-based nanostructures are also actively investigated [6]. It is now well established that the Si can absorb and emit visible light when its size is reduced to a nanometer scale below its excitonic Bohr radius ~5 nm. Gated three terminal devices made up of such Si_n nanoclusters are potential candidates to replace MOSFET in the

near future [4]. Hence it is very necessary to investigate an assortment of electronic structure dependent transport properties of these novel very small nanostructures in both bare and passivated conformations.

1.1 Nanostructured materials

A nanometer stands for a billionth (10^{-9}) part of a mater. In this length scale any solid of any shape is termed as a nanomaterial. Nanostructures refer to fabricated material systems having dimensions in the range of ~ 1-100 nm. At least one of their dimensions should comply with the nanoscale. In the nanostructure, electrons are confined in the nanoscale dimension(s), but are free to move in other dimension(s). For this reason, quantum dots (QDs), nanowires (NWs) and quantum wells (QWs) shows electron confinement in their three, two and one dimensions respectively. Another way of the classification of nanostructures is also based on the directions in which electrons move freely. Design and development of nanoscale material is just another step towards electronic device miniaturization. Physical, chemical, electrical and optical properties of these materials are often size and shape dependent [7].

1.2 Quantum confinement effect in nanostructures

Semiconductor nanocrystals having analogous interior bonding geometries compared to that of their known bulk counter parts exhibit distinct variations in their electrical and optical properties with size variation [8]. A core reason for these changes lies in a systematic transformation of the nanocrystal's density of states as a function of energy, start showing dependence on the nanoparticle's interior. From a density of state perspective, the nanocrystal lies in between discrete atomic and bulk limit. For any material there is an intrinsic size below which it exhibits a rough correspondence to an excitonic radius of the material and a fundamental blue shift in electronic and optical properties as a function of size. For the semiconductors another aspect of the size confinement is that on confining electron-hole pairs (excitons) in a small region of few nanometers in dimension, various electronic properties of the material gets entirely change. A order of magnitude of either the electron's or the hole's De Broglie wave length (λ) which is ~1nm, becomes comparable with confinement dimensions in nanoclusters. Hence the charge carriers in nanoclusters start behaving as particles in a box. Consequently, the confinement effect in a region of nanometric size is referred to as the quantum size effects (QSE) and the physical

structure, in which the quantum confinement of excitons occurs, is termed as the nanostructured material [9].

1.2.1 Brief details of various nanostructures

Progress in epitaxial growth and advances in patterning and other progressing techniques have made it possible to fabricate 'artificial' dedicated materials for microelectronics [10]. In these materials the electronic structure is tailored by changing the local material composition and by confining the electrons in nanometer size foils or grains. Due to a quantization of electron energies, these systems are often called quantum structures. Such quantized behavior is often manifested when the size becomes smaller than the Bohr's excitonic radius. The quantum confinement of excitons may occur in only one direction, in two directions or in all the three directions depending on the shape of the nanostructures. At each confinement direction there corresponds a radical change in the wave function of the particle and as a consequence, a series of discrete levels appear.

Quantum Dot: - A quantum dot has all the three dimensions in the nano range. This means, there is a total confinement in each direction and particles cannot move freely anywhere. Thus it is referred to as a 0-D nanostructure.

Quantum Wire: - is a 1-D nanostructure where particles are free to move in only one direction. Thus the two sides of the structure are of nanometer length.

Quantum Well: - A quantum well is a nanostructure where the two dimensions are available for movement of particles, while the third direction determines the quantum confinement direction. It is said to be a 2-D nanostructure [11, 12].

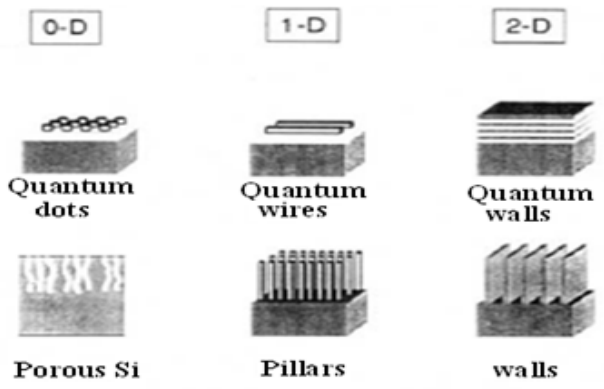

Figure 1 Silicon low dimensional structures of the semiconductors are shown as a schematics of quantum dots, quantum wires and quantum wells also known as nanoclusters, nano pillers and two dimensional nanowalls respectively [12]

The quantum dots can be obtained by means of different techniques such as chemical vapor deposition (CVD), Ion-implantation, sputter deposition, etc. The 1D structure or a quantum wire can be synthesized by depositing layers of different materials having nanometric dimensions; for example in Si/SiO_2 multipliers; SiO_2 layers act as a barrier, while excitons are confined in Si layers. A schematic given in figure 1 portrays various nanostructures classified in their corresponding dimensions.

1.2.2 Density of states in the view of quantum confinement

As a result of the quantum confinement in different directions, there is a change in the wave function of electrons and holes and consequently contributing states per unit energy, hence the density of states will changes as a function of energy E. Generally, the density of states depends on the dimension of the nano-structure and the corresponding wave vector dispersion. In the case of a bulk-material, the density of states increases with energy follows a parabolic law in respect to energy variation. Therefore in a three dimensional bulk-material, the DOS (ρ) is defined as the number of available electronic state per volume per unit energy E and it is given by:

$$\rho_{DOS}^{3D}(E) = \frac{1}{2\pi^2}\left(\frac{2m^*}{\hbar^2}\right)^{3/2}\sqrt{E}$$

In a case of the two dimensional nano-structure or a quantum well, a carrier movement is restricted to a plane and the third direction which is perpendicular to the plane usually determines the quantum confinement direction. This is often common in the case of semiconductor hetero-structures and super-lattices; the existence of 2DEG (two dimensional electron gas) at the AlGaAs/GaAs interface is a widespread paradigm of this effect. The DOS (ρ) for the 2D system is defined as the number of electronic state per unit area per unit energy and it is given by:

$$\rho_{DOS}^{2D}(E) = \frac{m^*}{\pi \hbar^2}$$

On further reducing the dimension of the system a quantum-wire is obtained. Examples of such one dimensional structures include nano-tube, semiconductor nano-wire, and nano-rods. Amongst the quantum-wires, the charge carriers are free to move in only one direction and the two sides are confined with the DOS (ρ) defined by the availability of electronic state per unit length per unit energy and it is written as,

$$\rho_{DOS}^{1D}(E) = \frac{1}{\pi \hbar}\sqrt{\frac{m^*}{2E}}$$

Finally for the zero dimensional system (quantum dot), the confinement is along all three dimensions and the DOS (ρ) becomes a delta function. In the 0-D (strong confinement) the electron are confined in their motion in all three directions [11, 12].

$$\rho_{DOS}^{0D}(E) = 2\delta(E - E_0)$$

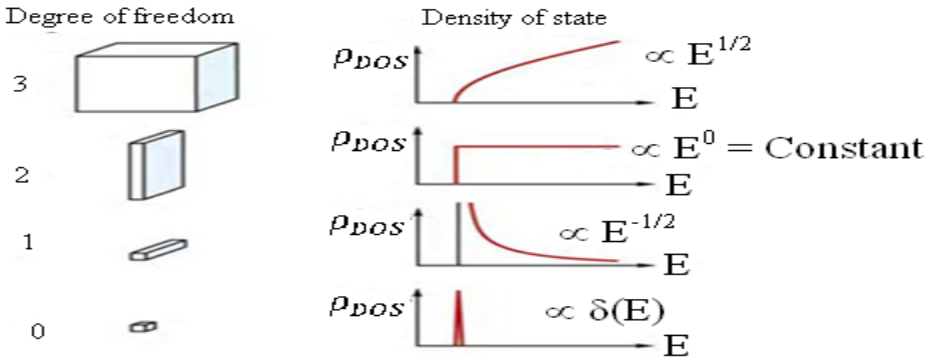

Figure 2 Electronic density of states of bulk and nanostructures semiconductors with 3,2,1,and 0 degrees of freedom [11, 12]

Properties of the nanostructures, such as, intrinsic conductivity, optical transitions, and electronic transitions mostly depend on the energy-gap between the Lowest Unoccupied Molecular Orbital (LUMO) and the Highest Occupied Molecular Orbital (HOMO) energy levels. These two energy levels act as the fundamental electron transition levels among the nanoclusters in anolofies to the molecular systems where these two levels corresponds to the bonding and antibonding levels of the principle transition. Any change of the gap may significantly alter the charge transport through the nanocluster. Miniaturizing a semiconductor for instance, down to a nanometer scale causes the band gap (E_g) to expand. The dielectric constant ε_r of the semiconductor is no longer constant but decreases with solid size. The reduced ε_r has enormous impact on the electrical and optical performance of the solid and the related devices [13]. This occurs when the width of a solid is reduced to the nanometer length scale. In addition to the size, effects such as structural changes, lattice contractions, surface passivation, atomic relaxation, surface reconstruction and local and non local strain induced by high surface energies can also change the gap.

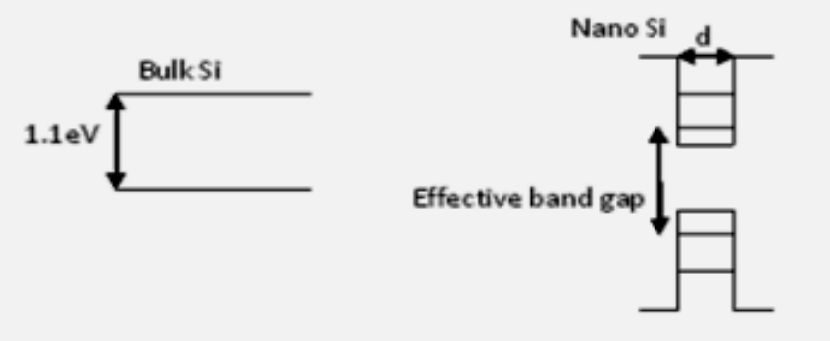

Figure 3 Energy band gap of the bulk Si system and that in the typical nanocluster. The presence of singularities in the DOS is easily discernable from the fland band electronic structure of the nanocluster [12].

1.3 Silicon nanoclusters

A nanocrystal is a single crystal having diameter of a few nanometers. Since the advent of advanced laser vaporization techniques semiconductor atomic and nanoclusters have become an active subject of research, both experimentally and theoretically. A great deal of understanding has been obtained on this microscopic form of matter, for example, their selectivity, stability, and reactivity, and their evolution toward the bulk matter. Silicon atomic and nanoclusters have been extensively studied because of their relevance to the development of nanoelectronics [8]. Small

silicon clusters display a rich variety of structures. It has been shown that embedded systems like that of Si/SiO_2 nanocrystalline quantum dots are also made up of very small silicon clusters completely embedded in the silicon dioxide [12]. These Si nanocrystals have already demonstrated the singularity signatures of ideal quantum dots due to carriers (electrons and holes) and phonons confinement. The ease of synthesis and processing of silicon nanoclusters due to recent advancements in the Si-Industrial technology make Si nanoclusters more attractive as a material of optoelectronic and functional devices. It has been reported that by using photo-oxidation, the size of Si quantum clusters can be precisely controlled by tuning the dosage of intense coherent light under a steady oxygen gaseous purging [14].

1.3.1 Novel Crystal Structures of very small Si nanoclusters

Very small silicon clusters display a rich variety of crystalline structures, which can be a square planer (pseudo two-dimensional) or distorted 3D crystalline forms. Such a variety of structures is truly absent in the bulk Si systems and originates only in a very small nano-si system owing to its very high surface energies and the dissimilar processes of energy minimization. These structures are neither open (chains, rings), like those of small carbon clusters, nor they are small fragments of the most stable bulk (diamond) silicon phase. Instead, the most stable Si_n clusters are usually compact, but they are not always quasispherical and high-symmetry structures. For instance, Si_6 is a tetragonal bipyramid, Si_7 is a pentagonal bipyramid and Si_8 is a distorted bicapped octahedron but Si_4 is a planar rhombus that is much more stable than any other tetrahedral isomer of the Si_4 cluster. The most stable six-, seven-, and eight-atom clusters common coordination numbers of well above 4.0 and are in hybridization states closer to s^2p^2 [15, 16]. Hence at present the studies of very small nanoclusters becomes an active and sizzling area of research. Many theoretical studies based on electronic structure calculations have previously attempted to tackle the problems of (1) predicting the relative stabilities of various Si_n isomers, and (2) providing a detailed electronic structure understanding [16]. In addition, a number of empirical models have also been developed for use in the simulation of condensed phases of silicon. These studies showed that it is very difficult, if at all possible, to devise a single classical potential that gives qualitatively correct descriptions of the bonding for vastly different arrangements of silicon atoms. Empirical models for silicon clusters are even more difficult than it is for surfaces and the

bulk, a number of such models have been failed recently [15]. Hence, at present only the ab-initio DFT techniques offer any viable modus operandi to comprehend these nano clusters.

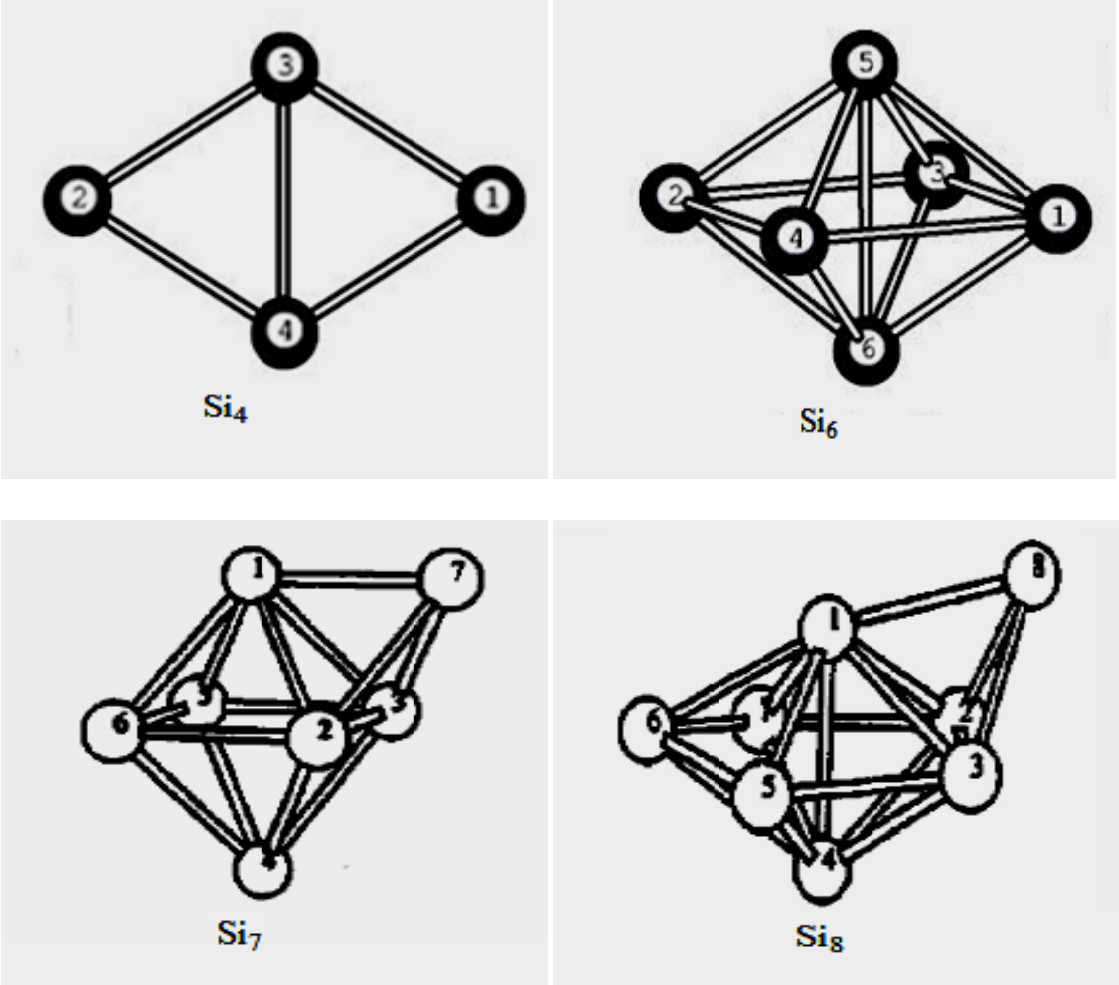

Figure 4 Cluster structural geometries for low-energy isomeric forms of the silicon nanoclusters corresponding to the magic number disparity [8, 16]

1.3.2 Properties of Silicon Nanoclusters (Si_n)

1.3.2.1 Optical Properties

In the early 1990s, quantum size effects (QSE) and the higher stability of very small Si clusters usher a new field of nonstructural silicon's research & development [10]. Through an electrochemical etching, the bulk silicon can be converted into the porous nanostructural form and it is found to show photoluminescence in the visible range. Soon the new effect is attributed

to presence of various silicon nanoclusters and nanowires amongst these nanocrystalline porous structures [16]. From the hybrid experiments of a scanning tunneling microscopy (STM) in conjunction with micro PL spectroscopic observations, it is estimated that the individual silicon particles display intense blue shifted photoluminescence. An explanation based on quantum size effects alone does not fully explain the photoluminescence (PL) observation. Surface species, structure stability, surface states, structural transformation and strain also play a crucial role in the appearance of such effects of energy blue shifts [17]. Efficient emission of visible light has been observed from the nanoclusters of silicon when they are exposed to ultra violet light. It is a well known fact that in a bulk Si system the indirect band gap of silicon causes a very long radiative lifetime (ms) for excited electron-hole pairs which allow the occurrence of various competing non-radiative recombinations and cause most of the excited electron-hole pairs to recombine non-radiatively. This yields very low internal quantum efficiency ($\eta \sim 10^{-6}$) for the bulk Si luminescence [18]. The production of red light in silicon nanocluster results from the electron-hole pair recombination across the band. The quantum confinement effect changes the energy level continuum in the bulk silicon into a discrete level structure namely the sub-band structure. This leads to the enhancement of the oscillator strength of the excitons through increased spatial overlap between the electron and the hole. The dielectric confinement also enhances the excitons binding energy and the excitons oscillator strength for nanoclusters having size of the order of exciton Bohr radius. From the electronic structures of the nano Si clusters systems, it has been observed that the nanoclusters have a direct band gap and emit light from violet to red depending up on the size of the structures [19]. It has also been found that with a large surface/volume ratio, the surface effects become more enhanced among these quantum confined systems. Therefore, geometry plays an important role in the electronic structural properties. Surface effects as well as quantum confinement effects are thus anticipated to control the optical and electrical properties of these materials.

1.3.2.2 Electrical Properties

The electrical transport properties of Si_n are determined mainly by its microstructures. With silicon nanocrystals embedded in ultra thin oxide by the rapid thermal oxidation (RTO) of an ultra thin chemical vapor deposition (CVD) amorphous Si (a-Si: H) film, some novel features such as the current peak and valley and the hystersis are revealed in I-V characteristics curve of

the diode structure. This suggests the charging of a definite amount of electrons at the silicon nanocrystals and the subsequent screening effect on the tunnel current [20, 12]. The experimental research on very small Si nano clusters in 2-probe devices also suggest the presence of negative differential resistance (NDR) in these clusters at specific bias windows.

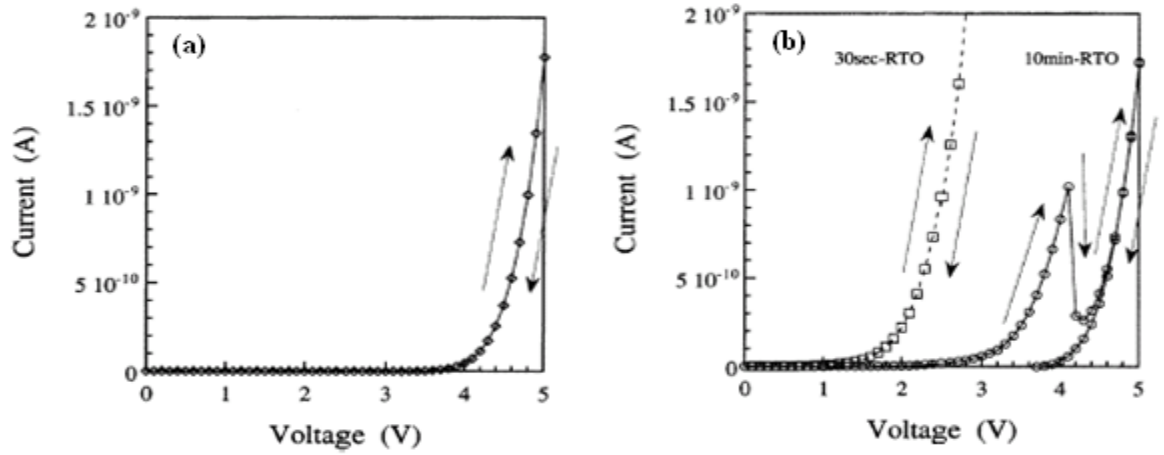

Figure 5 (a) Typical static I–V characteristics10 min-RTO diode sample, (b) Typical dynamic I–V characteristics of a 10 min (solid curve) and 30 s (dashed curve) RTO. Using vertically inverted arrow in figure-b it is shown that in the bias window of 3.5 V to 4-0 V the NDR phenomenon manifests in the form of decrease in current on increasing potential drop. [6]

1.4 Passivation of silicon nanoclusters

As discussed size-reduction of the semiconductor to the nanometer scale is apparently found to modify the physical properties of the material in a fundamental way. For example, silicon clusters with a diameter of a few nanometers exhibit an increased optical gap and narrower emission spectra compared to bulk values. In addition, the nanometer scale materials dimensions also cause a dramatic increase of surface area to volume ratio; therefore, the physical and chemical properties of silicon nanoclusters are greatly influenced by high surface energy induced effects like surface reconstruction, passivation, and surface related chemistry [21]. The presence of dangling bonds on the surface of silicon nanoclusters (Si_n) can be passivated by either hydrogen or oxygen. The size dependence of the effect of oxygen passivation on the optical properties of silicon nanoclustersis also previously carried out by using a single oxygen passivent atom. Nonetheless, among the silicon nanoclusters without oxygen contamination, the gap

increases as the size of the cluster decreases, thus demonstrating the quantum confinement effects. It is also shown before that amid the silicon nanoclusters with an oxygen contaminant, the HOMO-LUMO gap changes more swiftly than the gap of the purely hydrogenated clusters for clusters smaller than 1.8 nm [22]. As the Si nanocluster size increases beyond this critical 1.8-nm diameter, the fundamental HOMO-LUMO gap of pure hydrogenated silicon nanoclusters is found to decrease and the lowest gap is governed by the core transitions instead of the surface related transitions [22].

1.5 Nanoswitches and their working mechanisms

In designing a single molecule electronic switching device, it is highly desirable to understand the charge transport behavior for the nanocluster to function as an ideal transistor/switch, memory element, or as a chemical sensor. A figure 5 shows the conductance of a hypothetical single-channel device with well-defined on and off states. As depicted bottom line in the figure indicates a state of perfect insulator and a top line at 1 G_0 value of conductance indicates a state of perfect conductor. The fulfillment of this criteria represents a ballistic single-channel transport character of the nano-device, where the probability of back electron scattering within the nanocluster is negligible. Hence the nanoswitching device showing either of the upper and lower bounds of conductance can be termed as the perfect conductor and a perfect insulator respectively. As per se this definition the perfect switch should be a perfect insulator in the off state and a perfect conductor in the on state of the nano-device or vice versa (see Figure 5). Here it is interesting to note that these nanoclusters always have a nonconstant transmission probability as a function of energy due to the presence of singularities in their electronic density of states and the transmission is mostly dependent on the spatial separation of the singularities. Hence these small nanoclusters can be considered as a switch or transistor in which a change in bias or gate voltage leads to a change in the conductance. This peculiar property of the device can be usefully tapped in various switching related logic applications of futuristic nanodigital electronics. In general following are the criterions for the ideal switch: (1) an infinite ratio of the on current/off current (I_{on}/I_{off}); (2) a subthreshold swing of 0 mV/decade, indicating a switch that abruptly changes from the off state to the on state at a defined threshold voltage; (3) fast switching times that rely not on nuclear motion but only on changes in the relative electron density; (4) reproducibility and stability by minimizing charging and geometric organization; and

(5) low bias operation, energetically separated from a molecular resonance [23]. The small Si nanoclusters are projected to fulfill these ideal nanoswitch criterions satisfactorily

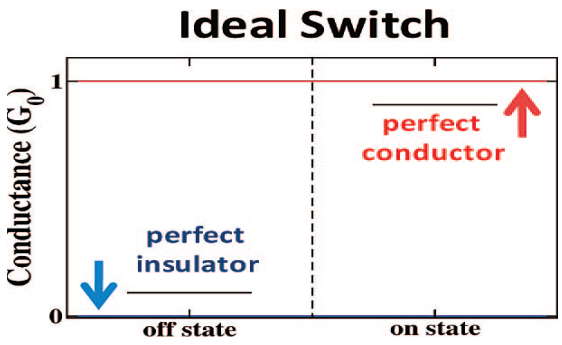

Figure 6 In an ideal switch, the off state would be a perfect insulator (bottom line at 0 G0), and the on state would be a perfect conductor (top line at 1 G_0). In a single transport channel, ballistic transport through a perfect conductor represents the on state of 1 G_0. Passivated Si_n nanoclusters are expected to act as ideal switch molecules due to their shape singularities expected in their quantum transport properties [24].

1.5 Graphene nanoribbon as an electrode material in a nanodevice

Graphene is an allotrope of carbon, whose structure is one-atom-thick planar sheets of sp^2 bonded carbon atoms that are densely packed in a honeycomb crystal lattice. It has shown great promise in many applications, such as nano-electronics, energy storage, supercapacitors, nano-batteries, hybrid fuel cells, nano BHJ solar cells and nanobiotechnologies. The Graphene is a single layer of graphite and it has attracted considerable research interests owing to its novel physical properties, such as massless Dirac fermion behavior, room-temperature quantum hall effect and high mobility. The two-dimensional (2D) graphene sheet itself is a semimetal. However, when the 2D sheet is cut into long rectangle slices, namely, the graphene nanoribbons (GNRs), they can become metallic or semiconducting depending on the zigzag or armchair pattern of crystallographic orientation. Hence the electronic properties of graphene can be easily tuned by cutting edges and the width of GNRs with a high degree of acerbic precision. Hence, GNRs possess tunable electronic bandstructure rendering the viability of GNR-based nanoelectronics devices [25, 26]. It is also to be noted that the as formed zigzag grapheme

nanoribbons (ZGNR) exhibits very high conductivities of the order of $>2G_o$, where G_o is the quanta of conductance. This is mainly owing to the presence of several charge transmission channels in the ZGNR.

1.7 Equilibrium conductance effects among nano-devices

Nanoelectronics two probe devices always have the small number of electrons and thus limited density of states in their nanostructural device elements. A typical theoretical or experimental nanodevice usually have a central region in nanocrystalline or molecular form that is atomically connected by the bulk external electrical leads. Such nano-devices rarely exhibit bulk effects like that of 'schottky barrier height' formation or other bulk band structure re-alignments. Instead the nano-devices have found to possess several novel mesoscopic effects which varies from the observance of fano resonant modes to strong coupling induced effects in between the three elements or regions of the device viz. left electrode, central region and right electrode (LCR). Such new effects are found to be sufficient to smear out various expected characteristics of their bulk counterparts. These new effects deal mostly with either the contribution of the electronic states from the electrodes to the central region (Si_n nanoclusters) resulting in the form of the fano resonance peak of the DOS and transmission spectra of the nano-device, or the coupling induced enhancement in the electron tunneling through the device which impediments the transfer of charge from electrodes to central region that results in the and resulting in the form of enhanced electron scattering in central nano-component [25]. These effects also manifest in the I-V measurements [26, 27] where the barrier is absent at the continuous-metallic/discrete-nanosemiconductor interface.

Nevertheless, when the injection of states from electrodes to central region is destructive in nature, we also have another possibility of observance of fano anti resonance dips in the DOS and in subsequent transmission spectrum at the Fermi level. This often results in a rectifying behavior of the nano devices [28, 29]. Hence nano device are not like bulk shottcky barrier or p-n junction switches but rectification in them arise either due to fano effects or due to singularities present in their DOS which in retrospect arise from the quantum confinement as described earlier [11, 12]. Moreover in the various atomistic ab-initio modeling, the bulk type electrical contacts are totally absent and purely atomic contacts are formed [29, 28]. This implies that the I–V

characteristics and rectification behavior (if any) in the device mainly depends upon (a) electrode materials and their dimensionality, whether they are one dimensional or two dimensional, (b) singularities present in the density of electronic states of the nanostructure located at the central region (sample to be tested) of the device, (c) interface and the contact geometry of the electrode and central region and (d) coupling strength between the two ends of the central region with the electrodes [30]. Often the strong coupling results in sharp and intense DOS peaks near the Fermi level and weak coupling gives broader DOS resonant states. This effect is also earlier reported in the density of states and transmission energy spectra along with I-V measurements [28, 29], where the ohmic like contacts are observed instead of rectification at the nanometallic/nano-semiconductor atomic interface.

Large values of equilibrium conductance, which is conductance at the Fermi level has previously been theoretically reported in case of 2-probe device simulations of Si_4 nanoclusters sandwiched in between Aluminum metallic electrodes [31]. The above mention novel size induced effects can only explain the existence of such large states. The high levels of equilibrium conductance also indicate the absence of schottky barriers in the nano-devices and it is mainly responsible for the ohmic character of I-V curves in these nano-devices. A number of authors have also attributed the significant equilibrium conductance to the charge transfer that occurs in between the electrodes and the central scattering region which increases low bias conductivity of nano/molecular devices [32]. Such charge transfers usually realign the LUMO of central scattering region with that of the Fermi level of electrode continuum conduction band that leads to large zero bias conductivity of the nano device [33]. In few earlier reports also it that been found that the increased charge transfer in between the electrodes and nanocluster changes strength of coupling and hence the as originated alterations in equilibrium conductance. On the other hand, rectification in a nano-switch largely dependent on such novel effects [34].

1.8 Objectives

1.8.1 General objectives

- To study very small semiconducting clusters (Si_n) and effects of passivation on their novel electronic properties
- To study Silicon nanoclusters (Si_n) in a nanodevice

1.8.2 Specific objectives

- To simulate electronic structures of Silicon nanoclusters in the passivated and bare states using the abinitio SIESTA code
- To investigate the charge density of states (DOS) and the transport in very small clusters of Si_4, Si_6, Si_7, and Si_8
- To simulate the I-V characteristics of nano-clusters sandwiched in between Graphene electrodes along with various nonequilibrium dynamics and nanoswitching properties.

Chapter Two

Simulational Methodology

The physical, chemical and electronic properties of nanomaterials are responsible for their potential applications in nanodevices. The study of electronic structure and transport properties of nanostructures has been a main field of research amongst the scientists since the advent of last decade. New theoretical method such as semi-empirical, first principle or ab initio, and density functional theory (DFT) have been developed for the systematic study of the electronic structure of nanomaterials. By the help of specifically developed user friendly software tools like TransSIESTA driven, ATK toolkit for nano electronics which is based on modern abinitio methods, we can investigate electronic structure as well as equilibrium and nonequilibrium transport properties in a systematic and controlled manner. The simulation and modeling features especially of ATK and VNL software are more versatile and useful especially in electronic and transport studies of nanoelectronic devices.

2.1 Brief review of modern theoretical methods

Quantum mechanics formulation provides the essential frame work for the study of nanomaterials electronic structure, in which the Schrödinger equation has to be solved to find the exact solution. This approach has been quite successful for single electron system but have some short comings and limitations when applied to determination of electronic structure of many body systems (i.e. the real crystals which are many electrons systems). The short comings of the approach are

- In many electron systems, the Schrödinger equation is solved for integration between nuclei and electrons which is a quite difficult process.
- Impossible to have the exact solution for many electron systems.
- Even if we solve and find the complete wave function of the crystal, it is difficult how to apply the function for the calculation of the physical properties.

The importance of the electronic structure study is to understand and predict the properties of many electron systems and to calculate several measurable quantities rather than solving simply the wave function. In order to attain these objectives and overcome the short comings mentioned above, the modern abinitio methods for electronic structure calculation are developed, are based on quantum mechanical frame work.

The three key processes involved in the calculation of electronic structures and transport properties are comprise of first principle self consistent calculations, density functional techniques (DFT) and exchange correlation add-ons, and NEGF for nonequilibrium charge dynamics.

2.2 Ab initio or first principle techniques

Ab initio is the Latin term for "from first principles", or, "from scratch". In ab initio methods, 100% of the modeling is done mathematically, based primarily on Schrödinger's equation. Using several constants, such as the speed of light and Planck's constant, the masses of the electrons and nuclei, etc we can develop and deploy the ab initio methods to calculate a wide variety of properties. The ab initio methods describe a complete mathematical approach to solve the Schrodinger equation for any material. In choosing the best ab initio methods specific for the desired problem in which nanomaterials are involved, one should have a proper choice of basis set that depends upon the shape and nature of involved electronic orbitals. At its most basic level, ab initio methods state that if one knows the structure of the material, one should be able to perform a complete calculation of that material completely from the mathematical principles with the aid modern computational tools. The Hamiltonian for a molecular system comprising N nuclei and n electrons is given by

$$\mathrm{H} = -\frac{\hbar^2}{2}\sum_{\mathrm{I}=1}^{\mathrm{N}}\frac{1}{\mathrm{M_I}}\nabla_{\mathrm{I}}^2 - \frac{\hbar^2}{2\mathrm{m}}\sum_{\mathrm{i}=1}^{\mathrm{n}}\nabla_{\mathrm{i}}^2 - \sum_{\mathrm{I}=1}^{\mathrm{N}}\sum_{\mathrm{i}=1}^{\mathrm{n}}\frac{\mathrm{Ze}^2}{\mathrm{r_{i,I}}} + \sum_{\mathrm{I}=1}^{\mathrm{N}}\sum_{\mathrm{J}=1}^{\mathrm{N}'}\left[\frac{\mathrm{Z_I Z_J e}^2}{\mathrm{r_{I,J}}}\right] + \sum_{\mathrm{i}=1}^{\mathrm{n}}\sum_{\mathrm{j}=1}^{\mathrm{n}'}\left[\frac{\mathrm{e}^2}{\mathrm{r_{i,j}}}\right]$$

In general, the Hamiltonian contains the following terms

where,

a) the nuclear kinetic energy term

$$-\frac{\hbar^2}{2}\sum_{I=1}^{N}\frac{1}{M_I}\nabla_I^2$$

b) The electronic kinetic energy

$$-\frac{\hbar^2}{2m}\sum_{i=1}^{n}\nabla_i^2$$

c) The electron-nuclear attraction

$$-\sum_{I=1}^{N}\sum_{i=1}^{n}\frac{Ze^2}{r_{i,I}}$$

d) The nuclear-nuclear repulsion

$$+\sum_{I=1}^{N}\sum_{J=1}^{N'}\left[\frac{Z_I Z_J e^2}{r_{I,J}}\right]$$

e) The electron-electron repulsion

$$+\sum_{i=1}^{n}\sum_{j=1}^{n'}\left[\frac{Z_I Z_J e^2}{r_{I,J}}\right]$$

Obviously, by looking at the complexity involved in the above Hamiltonian, the exact solution for more than one electron is impossible. Hence we use some approaches that effectively approximate and simplifies the problem for a number of nano-systems. One such scheme is known as density functional theory. [35]

2.3 The Density functional theory (DFT)

The study of the electronic structure in atomic and molecular systems is important, and it plays a major role in determining many properties of these systems such as ground-state energy, geometry of the system, vibration frequencies, absorption spectrum, and so on. The structural optimization can be obtained by knowing the electron density, which can be calculated as the solution of the Schrödinger equations formulated under Born-Oppenhiemer's charge-lattice decoupled motion approximation. The as obtained structural formulation is still difficult to solve for the real systems. Its exact solution is quite a challenge in quantum mechanics. However the de-coupled Hamiltonian can give useful results by a recently developed unique approach known as the Density Functional Theory, which came after its predecessor called as Hartree-Fock approach, when Hohenberg and Kohn published their theorem in 1964 [36]. The Hohenberg-Kohn theorems relate to any system consisting of electrons moving under the influence of an external potential $v_{ext}(r)$ and can be stated simply as follows:

- The ground-state energy of a many-body system is a functional of the electron density, n(r).

$$E_{Gs} = E[n(r)]$$

- The functional $E[n(r)]$ has its minimum at the equilibrium density n_0(r).

$$E_{GS} = E[n_o(r)] = \min\{E[n(r)]\}$$

Pseudopotential or **effective potential** is used as an approximation for the simplified description of complex systems. It is an attempt to replace the complicated effects of the motion of the core (i.e. non-valance) electrons of an atom and its nucleus with an effective potentials, or pseudopotential, so that the Schrödinger equation contains a modified effective potential term instead of the coulombic potential term for core electrons normally found in the Schrödinger equation. **Plane wave** is a constant-frequency wave whose wave fronts (surfaces of constant phase) are infinite parallel planes of constant peak-to-peak amplitude normal to the phase velocity vector.

2.4 Kohn-Sham Scheme

The Kohn-Sham approach is one of the important approaches in density functional theory and was discovered by Kohn and Sham in 1965. They started their approach by introducing the ground-state wave-function of the non-interacting Fermionic system. Thus,

$$\Theta = \frac{1}{\sqrt{N!}} \begin{vmatrix} \varphi_1(\vec{x}_1) & \varphi_2(\vec{x}_1) \dots & \varphi_N(\vec{x}_1) \\ \varphi_1(\vec{x}_2) & \varphi_2(\vec{x}_2) \dots & \varphi_N(\vec{x}_2) \\ \vdots & \vdots & \vdots \\ \varphi_1(\vec{x}_N) & \varphi_2(\vec{x}_N) \dots & \varphi_N(\vec{x}_N) \end{vmatrix}, \quad 1$$

Where φ is called the one-electron orbital, and it is a function of the spatial-coordinate and spin coordinate of the electron. It can be determined from the following Kohn-Sham equation.

$$\hat{f}^{KS}\,\varphi_i = \varepsilon_i \varphi_i \quad 2$$

Where the quantity $\hat{f}^{KS}$ is the Kohn-Sham operator, which consists of two operators which are the kinetic energy operator and the potential operator as we put into the equation below:

$$\hat{f}^{KS} = T_s + V_s \quad 3$$

Then, by using the electrons orbitals we obtained from the set of Eqn. (2), we can define the ground-state density $n_s(\vec{r})$ of the non-interacting system.

We assumed this density equal to the ground-state density of the interaction Fermions system $n(\vec{r})$, which surmises our theoretical framework. It is to be noted that this assumption is accompanied by the incorporation of another density dependent function that is described in the next section, therefore, [37]

$$n_s(\vec{r}) = \sum_i^n \sum_s |\varphi_i(\vec{r}_i, s)|^2 = n(\vec{r}). \qquad 4$$

2.5 Approximation for Exchange-correlation function

The exchange-correlation term is an important part in the density functional calculation because this accounts for all the mutual electronic interactions and extensively used for performing any practical calculation with its approximate. There are many functionals developed to approximate this term, and all these functionals are developed from the electron density of the uniform gas (the gas which has a constant density), Therefore, we shall concentrate only on one of the accurate exchange-correlation functional which is **Local Density Approximation (LDA)**. The LDA has a simple prescription which is given by,

$$E_{xc}^{LDA} = \int n(\vec{r}) \in_{xc} \left(n(\vec{r})\right) d\vec{r}$$

$\in_{xc}$ represents the exchange correlation energy per electron, and $\in_{xc}$can be expressed by two terms, which are exchange and correlation contributions, given by the following form

$$\in_{xc} \left(n(\vec{r})\right) = \in_x \left(n(\vec{r})\right) + \in_c \left(n(\vec{r})\right)$$

$\in_x \left(n(\vec{r})\right)$ represents the exchange energy for the one electron, in the uniform electron gas with the density $n(\vec{r})$. It is given by [38]

$$\in_x \left(n(\vec{r})\right) = -\frac{3}{4}. \sqrt[3]{\frac{3n(\vec{r})}{\pi}}$$

2.6 Non-equilibrium Green's function technique

The nonequilibrium Green function (NEGF) method potentially has several advantages to investigate electronic transport properties of nanoscale materials such as single molecules, atomic wires, carbon-based materials, and thin layers in device configurations. The potential advantages are summarized by the following features of the NEGF method: (i) the source and drain contacts are treated based on the same theoretical framework as for the scattering region; (ii) the electronic structure of the scattering region under a finite source-drain bias voltage is self-consistently determined by combining with first-principles electronic structure calculation methods such as the density-functional theory (DFT) and the Hartree- Fock (HF) method; (iii) many-body effects in the transport properties, e.g., electron-phonon and electron-electron interactions, might be included through self energies without largely deviating the theoretical framework; (iv) its applicability to large-scale systems can be anticipated since the NEGF method relies practically on the locality of basis functions in real space, resulting in computations for sparse matrices. Due to those potential advantages, recently several groups have implemented the NEGF method coupled with the DFT or HF method using atomic type or the other local basis functions with successful applications for calculations of the electronic transport properties [39].

The current-voltage (I-V) characteristics is given by

$$I = \frac{2e^2}{h} \int T(E, V_b) \, [f_l(E) - f_r(E)] dE$$

Where $T(E, V_b)$ is the transmission coefficient at energy E and bias voltage V_b. The Fermi distribution functions $f_{l/r}(E)$ limit the integration to a small energy range eV_b at the Fermi level of the electrodes.

2.7 Quasi-Newton structural optimization method

Quasi-Newton is one of the molecular dynamical (MD) algorithms which we have used for geometrical optimization of various Si_n nano-cluster conformations. This algorithm works on the principle of finding local maxima and minima of coulambic forces. Quasi-Newton methods are based on Newton's method to find the stationary point of a function E(x); where the gradient is zero. Quasi-Newton's method assumes that the function can be locally approximated as a

quadratic in the region and iteratively optimized by using its first and second derivatives to find the stationary point.

$$E(x) = E(x_0) + g\Delta x + {}^{1}/_{2}\,\Delta x H_0 \Delta x \qquad 1$$

Differentiation with respect to coordinate yields

$$g(x) = g_0 + H_0\Delta x \qquad 2$$

Where E(x) is potential energy

g_0 is the gradient $\left({}^{dE}/_{dx}\right)$ at x_0

H_0 is the Hessian matrix, which is the square matrix made up of the second order partial derivatives $\left({}^{d^2E}/_{dx^2}\right)$ at x_0 of the function E(x) and $\Delta x = x - x_0$

At the stationary point, the gradient is zero, $g(x)$=0 and the displacement is minimum given by

$$\Delta x = -H_0^{-1} g_0 \qquad 3$$

Newton and Quasi-Newton methods are most efficient and widely used procedures for optimizing equilibrium geometries and also to find the transition structures [40]. In Newton method the Hessian in Eqn.3 is calculated at the current point but in Quasi-Newton method we use the approximate Hessian that is updated at each step of the optimization. Because the actual potential energy surfaces are rarely quadratic, several Newton and Quasi-Newton steps are require to reach a stationary point. For minimization, the Hessian must have all positive eigen values (i.e., positive definite). If one or more eigen values are negative, the step will be taken toward a 1st or higher-order point. Quasi-Newton methods start with a crude geometrical structure based on the predicted material's atomic structure, which yields our approximate Hessian. The difference between the calculated change in the gradient and the change predicted with the as approximated Hessian is further used to improve the Hessian at each step during the optimization routine.

$$H^{new} = H^{old} + \Delta H \quad (4)$$

For a quadratic surface, the updated Hessian must fulfill the following Newtonian condition,

$$\Delta g = H^{new}\Delta x \quad (5)$$

Where $\Delta g = g(x^{new}) - g(x^{old})$ and $\Delta x = x^{new} - x^{old}$.

There are an infinite number of ways to update the Hessian and fulfill the Newton condition. Symmetric rank one (SR1) update is one of the simplest update and also known as the Murtagh–Sargent update.

$$\Delta H^{SR1} = \frac{(\Delta g - H^{old}\Delta x)(\Delta g - H^{old}\Delta x)^T}{(\Delta g - H^{old}\Delta x)^T \Delta x} \quad (6)$$

If $|\Delta g - H^{old}\Delta x|$ is very small the formula will encounter many problems. We can also use another update method to solve the problem that occur in SR1 called Broyden-Fletcher-Goldfarb-Shanno (BFGS). BFGS update is the most successful and widely used in recent calculations.

$$\Delta H^{BFGS} = \frac{\Delta g \Delta g^T}{\Delta g^T \Delta x} - \frac{H^{old}\Delta x \Delta x^T H^{old}}{\Delta x^T H^{old} \Delta X} \quad (7)$$

As we discussed the Quasi-Newton methods require an initial estimate of the Hessian. A scaled identity matrix may be sufficient in some cases, but a better starting Hessian can be obtained from the atomic structure and atomic bonding pattern of the as modeled nanocluster [40].

2.8 The SIESTA software package

SIESTA (Spanish Initiative for Electronic Simulations with Thousands of Atoms) uses self-consistent density functional theory (DFT) for the calculation of the electronic structure. In addition to this, it offers options to modify the nuclear variables, such as molecular dynamics simulations, optimization and phonon calculations. It uses a linear combination of atomic orbitals (LCAO) as basis set. There is a choice of direct solver or iterative solver for the eigenvalue problem. The iterative solver scales linear with the number of atoms [41].

ATOMISTIX TOOLKIT is a library of atomic scale modeling techniques that can be used to calculate a wide range of properties of nanoscale systems. Its most unique feature is the ability to calculate the electrical properties of nanoscale devices, which consist of a scattering region coupled to two macroscopic bulk systems or electrodes. Atomistix provides two different interfaces for performing electronic transport calculations:

- VIRTUAL NANOLAB (VNL) which is a graphical user interface (GUI)
- I-python which is non-GUI ATK interface. This is a file-based or command line interface.

Most users will probably find the VNL as an appealing option, because of its intuitive ease of use. Some prefer non-GUI ATK interface because it is faster, transparent, gives more control and calculations can be automated by using scripts. Moreover, I-python provides immediate access to the newest functionalities.

Our modeling study generally consists of three parts: setting up the calculation, running the calculation and finally analyzing the output of the calculation [42]. When setting up a calculation, the first thing to consider is the symmetry of the system. ATK provides methods for describing three different system types; molecular, bulk, and two-probe systems. A two-probe system consists of a nanoscale region coupled to two macroscopic bulk systems, or electrodes. The nanoscale region can be a molecule, nanotube, cluster of atoms, a piece of a semiconductor or an interface between the electrodes. The way we work with VNL is in many aspects similar to what we would do in an actual experiment:

- First we set up our system using either of the Molecular Builder, the Crystal Cupboard, or the Atomic Manipulator tools.
- After setting up our system (theoretical sample), we specify the details of the DFT method that should be applied to our system. We do this using either the Method Editor or the NanoLanguage Scripter tool.
- Once the DFT method has been defined, we select the physical properties that should be extracted from the calculation. We do this by using the NanoLanguage Scripter tool.
- The calculation is then performed by submitting the job to the Job Manager tool or executing it from the command line.
- Finally, we analyze and inspect the obtained data by using the Nanoscope and the Result Browser tools.

In short, VNL is designed to bridge experimental and computational approaches by offering a spectrum of useful tools for performing virtual experiments. The NanoLanguage scripts that are generated with VNL are performed with the Atomistix ToolKit (ATK) calculation engine.

On launch Virtual NanoLab (VNL), the first thing which appears is the VNL Toolbar window [43].

The Toolbar provides access to all the individual tools that are used in VNL.

Tool	**Icon**	**Description**
Atomic Manipulator		Set up two-probe systems and make modifications to two probe device
Molecular Builder		Build and construct your own molecules ready to be used in other VNL tools
NanoLanguage Scripter		Create complete calculation set-ups and store these as Nano-Language script
Method Editor		Predefine DFT and NEGF parameters for reuse in the Nano-Language Scripter when generating NanoLanguage scripts.
Script Editor		Manually edit and extend NanoLanguage scripts constructed by the different set of VNL tools.
Job Manager	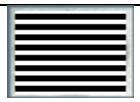	Execute scripts using the ATK computation engine.
Nanoscope		Visualize atomic geometries and calculated properties in 3D
Result Browser		Browse the contents of VNL files including all stored samples and results within them.

Table1 Various modules of the Siesta based Atomistix toolkit software package under the Virtual Nanolab GUI interface. We have deployed these tools for the theoretical simulation of our as modeled Si nanoclusters.

Chapter Three

Details of Simulational sample preparation

3.1 Steps involved in the Si_n nanocluster construction

We can prepare the simulational samples by the help of a SIESTA based ATK toolkit software. Following steps are very useful for the theoretical synthesis of highly stable very small Si nanoclusters samples and their theoretical nanoswitches.

- Start VNL software package which is a GUI or front-end of Atomistix abinitio DFT code.
- In the Molecular Builder we can model our samples with the help of the Geometry manager, Molecular Cupboard and periodic table (see Figure 7).
- After modeling the rudimentary Si_n (n=4, 6, 7, 8) sample with the help of the molecular builder by using standard atomic structure obtained from the literature [8, 16], drop it to the NanoLanguage Scripter then create complete calculation by using appropriate geometric optimization parameters, set-ups and store this as a Nano- Language script and finally we execute scripts using the ATK computation engine and standard commands syntaxes. This would give us the configurationally optimized sample for different compositions of Si nanoclusters. The resulting sample's geometric xyz files are saved as .py extension.

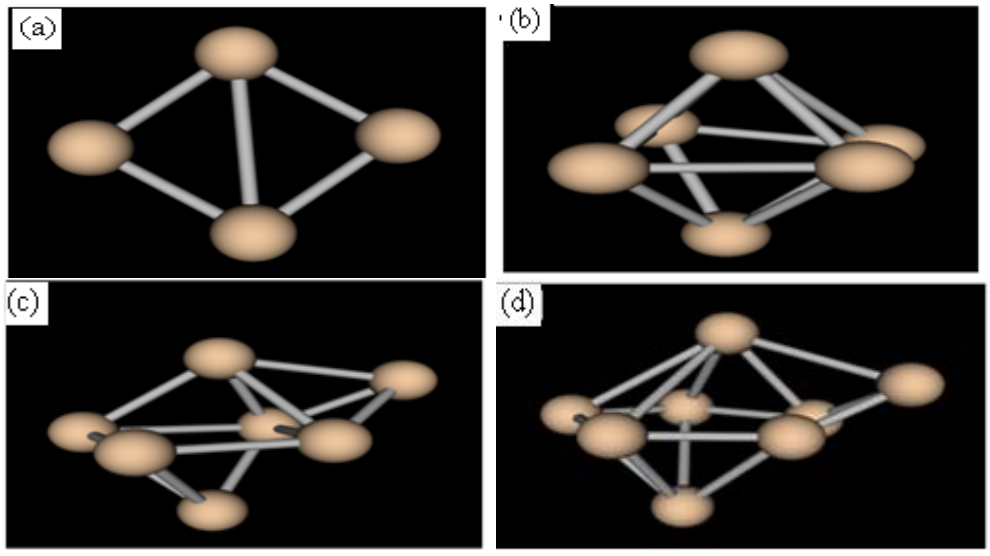

Figure 7 The schematic diagram unoptimized of (a) Si_4, (b) Si_6, (c) Si_7, and (d) Si_8 nanoclusters. The used structure coordinate values are taken from the literature as described in the text.

3.2 Steps involved in the Si_n nanocluster structural optimization

In the optimization process we do the following procedures. First drop the unoptimized structure from molecular builder to NanoLanguage scripter, second in the NanoLanguage scripter on the geometry optimization set Quasi-Newton optimization. In Quasi-Newton optimization method we can set and define the parameters of force tolerance value of 0.02eV/Angstrom, max step or iteration size of 200 and trust radius of 0.5 Angstrom, and create programs for a set of calculations and finally execute the script. This ensures the correct optimization of the structures of magic numbered nanoclusters. Finally, we visualize the as optimized structures by usinga molecular builder or a nanoscope, which are shown in a figure 8. The sample preparation procedure is terminated by the NanoLanguage scripter that performs the set up of certain calculations to find the energy spectrum and transport of the optimized structures directly from the ATK command console.

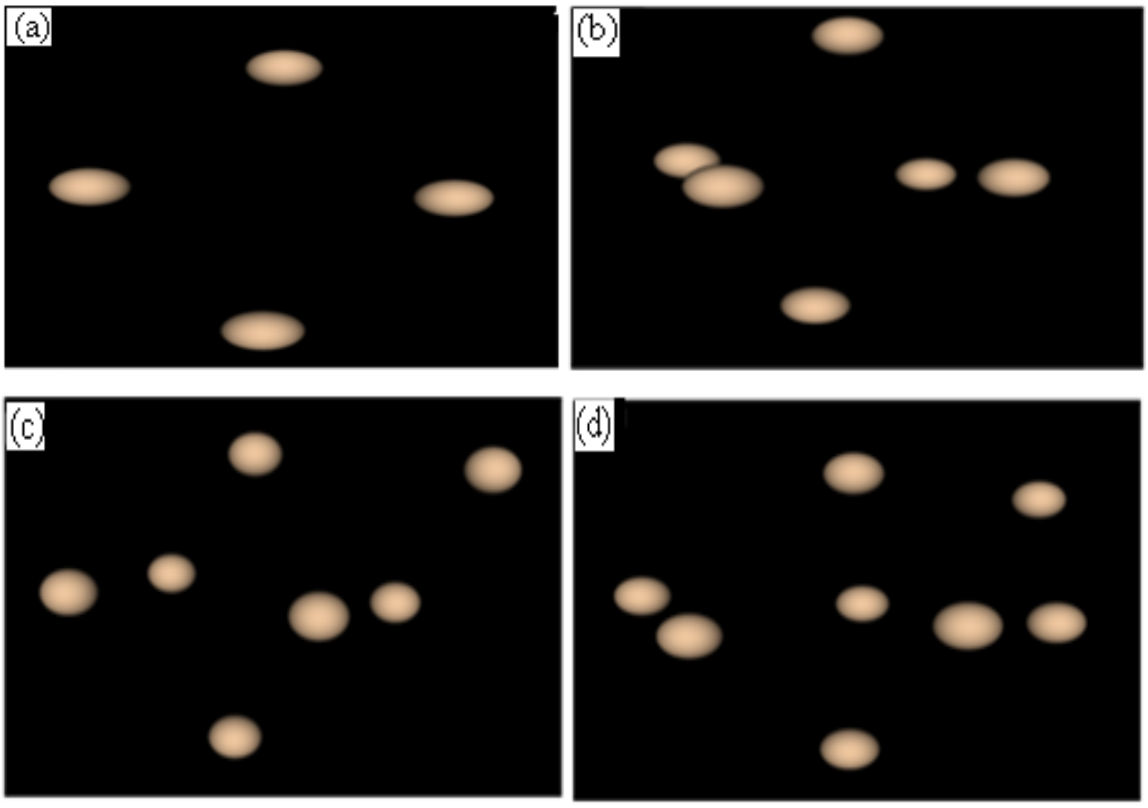

Figure 8 The schematic diagram optimized of (a) Si_4, (b) Si_6, (c) Si_7, and (d) Si_8 the structures are found to be comparable with the reported crystal structures prevalent among them as discussed in the text.

In the Nano- Language script we set different parameters such as specify the check file name, analysis and method. In the method we set the parameters as follows;

Basis set parameters	Type	Single zeta
	Energy shift	0.01 Rydberg
	Delta Rinn	0.8
	V_0	40 Rydberg
	Split Norm	0.15
	Radial Sampling DR	0.001 Bohr
Brillouin zone integration parameters	Number of k-points (A)	1
	Number of k-points (B)	1
	Number of k-points (C)	500
Eigen State Occupation	Left electrode-electron temperature	300 K
	Rightelectrode-electron temperature	300 K
Electrode Voltage	Left Electrode	0 Volt
	Right Electrode	0 Volt
Electron Density	Mesh Cut-off	Central 150 Rydberg
Energy Counter integral parameters	Circle Points	30
	Integral lower bound	3 Rydberg
	Fermi Line Points	4
	Real Axis infinitesimal	0.01 eV
	Real Axis Point Density	0.02 eV
Exchange Correlation Functional	LDA.Pz (Perdew–Zunger functional)	
Iteration Control	Tolerance	1e-005
	Criterion	Total Energy
	Maximum Steps	500
Iteration Mixing	Quantity	Hamiltonian
	Diagonal Mixing Parameter	0.1
	Algorithm	Pulay
	History Steps	6
Two center Integral Parameters	Points	1024
	Cut-Off	2500 Rydberg
Two Probe Algorithm Parameters	Electrode Constraint	Off
	Initial Density Type	Equivalent Bulk

Table 2 Parameters used in the ab initio calculations of electronic and transport properties are shown in a tabular format

Some of the basic parametric terms can be described as follows;

- Single-zeta

  There are two general categories of basic sets;

  - ✓ Minimal basic sets (single-zeta)

    A basis set that describes only the most aspects of the orbitals. It takes less time as compare with the double-zeta.

  - ✓ Extended basis set (double-zeta, triple-zeta, and quadruple-zeta)

    A basis set with much more detailed description. It takes more time. Since it incorporates various radial and polarization informations about the atomic orbitals.

- Brillouin zone integration: - the total energy smoothly varying as of K-points. The K-sampling varies with the orbital shape and size.
- Mesh cut-off:- It's an energy (default 150 Ry) which corresponds to the fineness of the real-space grid on which the Poisson equation is solved.
- Cut-off is an arbitrary maximal or minimal value of energy, momentum, or length, used in order that objects with larger or smaller values than these physical quantities are ignored in some calculation.

Chapter Four

Results and discussions

In this chapter we are mostly concerned with the presentation of our as obtained simulational results from the atomistic calculations performed on the Si_n nanoclusters. The results comprise of the electronic structures of various nanoclusters followed with the other results of density of states, Transmission spectrum and I-V measurements which are performed in a 2-probe nano-device geometry. In all the samples we have taken a zigzag graphene nanoribbon as the left and right electrodes to ensure the minimal charge carrier scattering from the electrodes. Hence, the before mentioned excellent charge transport properties of graphene ZZ ribbons ensures this during the experiments.

4.1 Electronic structures of bare, hydrogen and oxygen passivated Si_n nanoclusters (n = 4, 6, 7 and 8)

A figure 9 (a-d) shows the band gap energy of unoptimized and optimized crystal structure of Si_4, Si_6, Si_7 and Si_8 nanoclusters correspondingly. Their pictorial representations are already given in the figures 7 and 8 showing the rhombus, tetragonal bipyramid, pentagonal bipyramid and distorted bicapped octahedron crystal structures respectively of the unoptimized and the optimized Si_n. The band gap energy of optimized structures of Si_4, Si_6, Si_7 and Si_8 are 1.25 eV, 0.45 eV, 0.65 eV and 0.43 eV and unoptimized structures are 4.67 eV, 1.48 eV, 3.49 eV and 0.81eV respectively. The optimized band gap-energy of Si_n clusters agrees very well with the band gap-energy calculated by G. Sashidhar *et al.* [44]

Si_n clusters	Si_nH clusters	Si_nO clusters	Total energy Si_n (eV)	Total energy Si_nH (eV)	Total energy Si_nO (eV)
Si_4	Si_4H_2	Si_4O_2	-704.535	-734.834	-1599.937
Si_6	Si_6H_2	Si_6O_2	-1059.583	-1087.823	-1954.520
Si_7	Si_7H_2	Si_7O_2	-1235.942	-1264.692	-2131.252
Si_8	Si_8H_1	Si_8O_1	-1413.576	-1427.369	-1866.500

Table 3 The total energies of bare, hydrogen and oxygen passivated of Si_n clusters

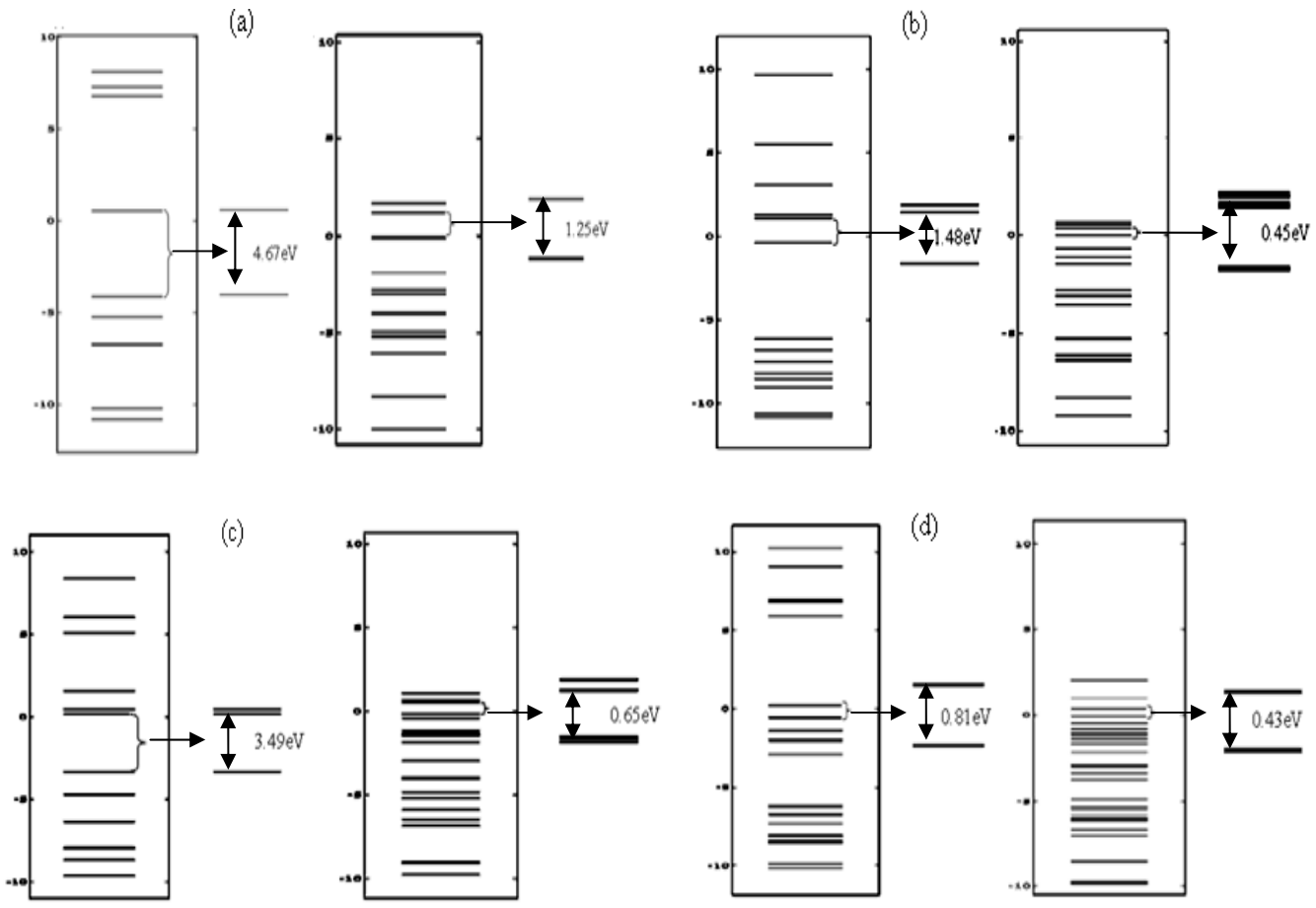

Figure 9 Flat band energy spectrum of unoptimized (left) and optimized (right) structure of (a) Si_4, (c) Si_6, (d) Si_7 and (d) Si_8 nanoclusters. All the spectra are Fermi energy corrected and zero point represents the Fermi position. A curly brace place on the band diagram represents the HOMO-LUMO gap and the corresponding energy gap values are written and shown by the arrow marks in both the unoptimized and optimized Si nanoclusters.

As we see from figure 9 (a-d) the number of available energy levels below the Fermi levels are more as compared to that of above Fermi level energy (E_f). Hence in our calculation we have obtained an asymmetric energy level distribution around the Fermi level. An electronic energy band gap structure of Silicon nanoclusters (Si_n) are represented such that the Fermi level E_f is deliberately set to zero point to avoid the inconsistency of the sign of the Fermi energy value. It

is to be noted that some ab initio codes generate the negative values of Fermi energy. The levels below the zero point are indicative of hole state and above corresponds to that of the electrons.

To examine the sample stability we have calculated the total energy of the modified Si_n, Si_nH and Si_nO cluster. The total energy of Si_n as well as Si_nH and Si_nO clusters decreases approximately linearly with the cluster size. Our simulations show that the addition of hydrogen and oxygen can cause large changes in the electronic structure of the host Si_n cluster because both the oxygen and hydrogen are more electronegative than the silicon and there is a charge transfer from the silicon atom to the oxygen and hydrogen atoms on passivation. The electrons are more localized near the oxygen and hydrogen atom. The total energy values as given in a Table 2 show that oxygen passivated clusters are geometrically more stable than hydrogen passivated Si_n clusters, and hydrogen passivated Si_n clusters are geometrically more stable than the bare Si_n clusters, this fact is also clearly depicted in a figure 10. Broadly, we have found that the stability of the clusters do not alter significantly with the hydrogen passivation but increases appreciably with the oxygen passivation. We ascribed such behavior in Si_nO to the higher electronegativity of oxygen atom, which confers charge transfer from cluster to the passivent atom, such behavior is also well exemplified from the figure 10.

Figure 10 Total energy minima from the modified geometries of Si_n nanoclusters in comparison with the number of silicon atoms present in the clustersand the type of the passivants attached to the nanoclusters.

In summary, the as obtained energy band gaps for the optimized samples of the Si_n nanoclusters are found to be varying in the range of 1.25 eV to 0.43 eV from lowest size to largest size of the nanocluster in the present set of studies. Such results can be explained firstly by the general trend of decreasing energy gap with the augmentation of the number of atoms (n) in the nanocluster. The reason for this trend can be ascribed to increase in stability of the cluster along with reduced quantum confinement effects on increasing size (i.e. n). It is to be noted that all the energy gap values for these small nanoclusters are less than that of the bulk silicon, which is spectrally positioned at 1.13 eV for a Si-diamond cubic bulk structure. Secondly, as explained previously the reduced energy gaps in nanoclusters are indeed due to their unique crystal structures that are very different from their bulk counterparts, which also brings enhanced stability in Si nanoclusters. Nevertheless, the exceptionally lower energy gap of Si_6 can also be attributed to the fact that structural total energy, which is also the indicator of structural stability, is lowest in Si_6 in comparison to Si_4 and Si_7. For an ascending order of cluster sizes, the values of average total energy per Si atom are -176.133 eV, -176.597 eV,-176.563 eV and -176.697 eV respectively. Therefore, due to enhanced stability of Si_6 nanoclusters, it is expected that the π orbitals in this nanocluster have significant extent of overlapping and hence we see an incomparable reduction in its gap in contrast to that of its closest neighbor, which is Si_7.

4.2 Silicon nanoclusters in a two probe device

Now we are in a position of designing a two probe device configuration, our two probe device contains central region, left and right electrodes. The central region of our two probe device comprises of the Si_n nanoclusters under consideration and the right and the left region are the two graphene nanoribbon electrodes connected to the device for applying the finite or sweeping bias across the nanoclusters. The sweeping bias window is set in between -2V to 2V in most of the cases to study the nonequilibrium physical properties of the nanoclusters. While the equilibrium conductance, density of state and transmission spectrum as functions of energy are calculated by keeping the value of the finite bias of 0V. Such left and right graphene electrodes connected to nanoclusters are used to inject the electrons from the left side to the central region and the holes injection (if any) takes place from the right Graphene electrode. Choice of zigzag Graphene

nanoribbon as a material of electrode in our device is based on their higher stability, high conductance and mobility and the ease of coupling with the central region.

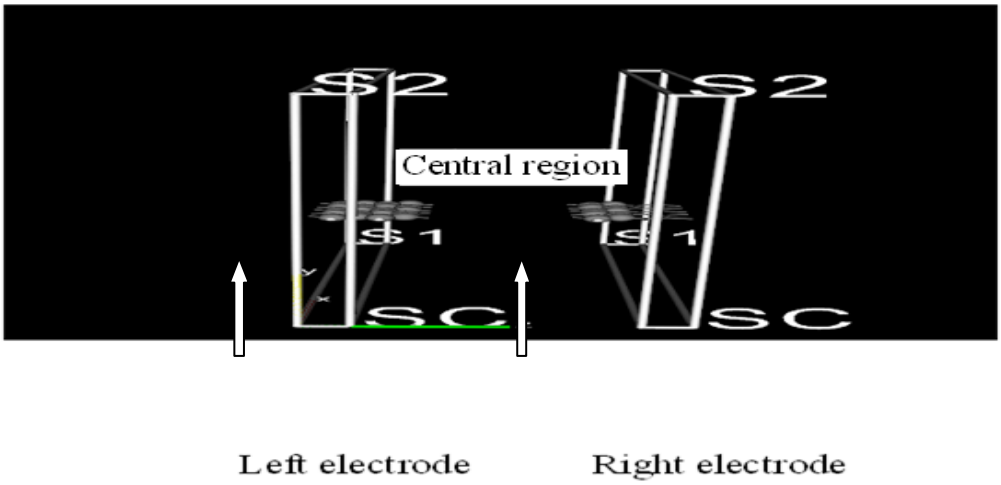

Figure 11 The schematic of an illustration of two probe device of graphene nanoribbon. The as modeled Si_n nanocluster is placed in the central region of the device and electrons are injected from the right graphene electrode and collected from the left graphene electrode.

We apply our scheme to silicon nanoclusters connected to two semi-infinite graphene ribbon leads, as shown in figure 12(a-l). The graphene ribbon leads are zigzag graphene nanoribbon, abbreviated as ZGNR. The central region and the electrodes are equally important for the transport properties. If either of the electrode or the central region is isolated, the current will flow by tunneling. In ATK, a central region combined with electrode constitutes a complete device configuration. A wired box in the figure 11 represents the atoms of the graphene which are repeated to a semi infinite structure and also represents the size of a solution domain used by transport calculation.

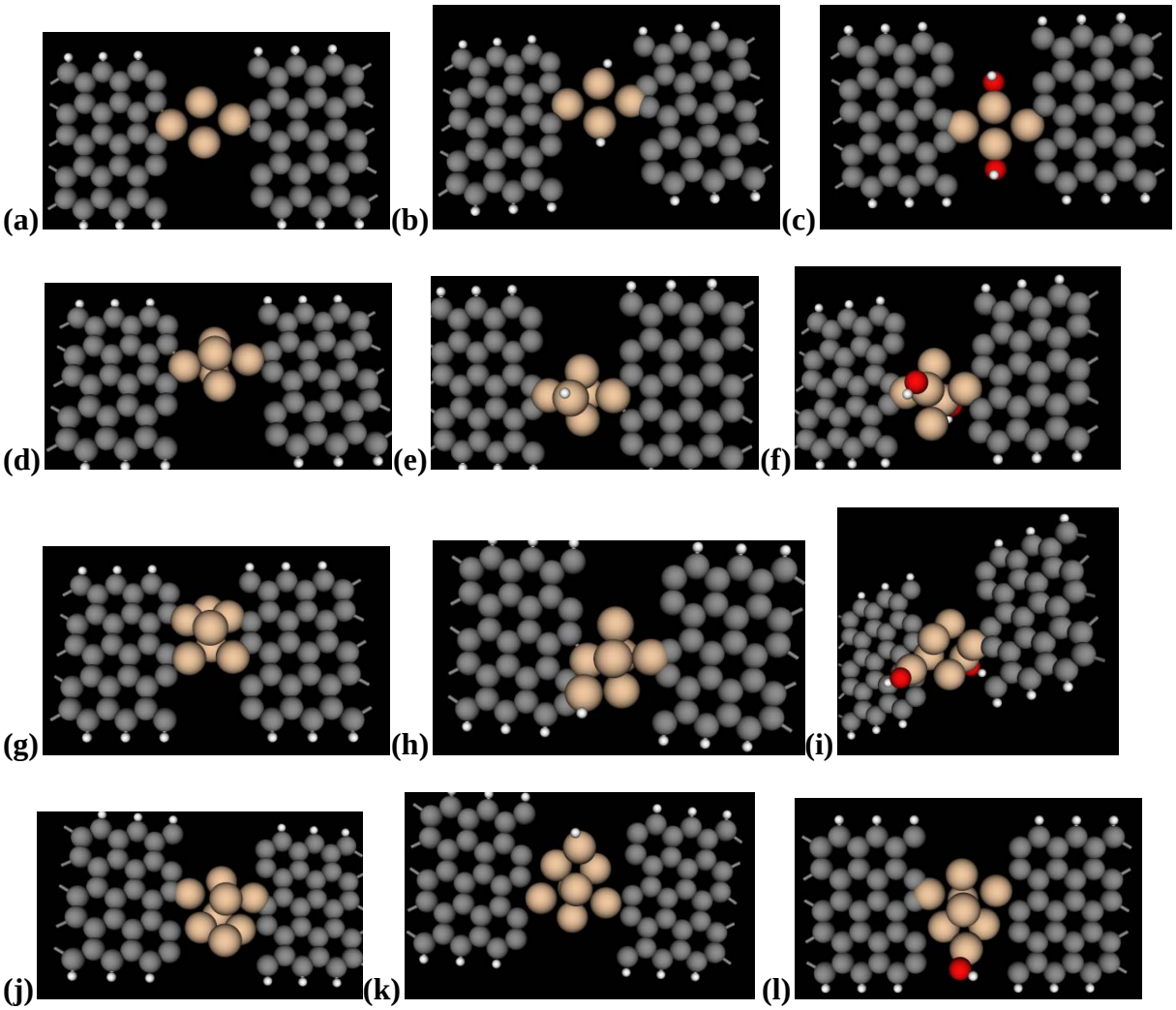

Figure 12 Schematic diagrams of two probe systems. Metallic zigzag graphene nanoribbon are used as the left and right semi-infinite electrodes which are bridged by the nanoclusters present in the central region comprises of (a) Si_4, (b) Si_4H, (c) Si_4O, (d) Si_6, (e) Si_6H, (f) Si_6O, (g) Si_7, (h) Si_7H, (i) Si_7O, (j) Si_8, (k) Si_8H, and (l) Si_8O clusters.

4.3 Density of states of bare and passivated Si_n (n=4, 6, 7 and 8) clusters

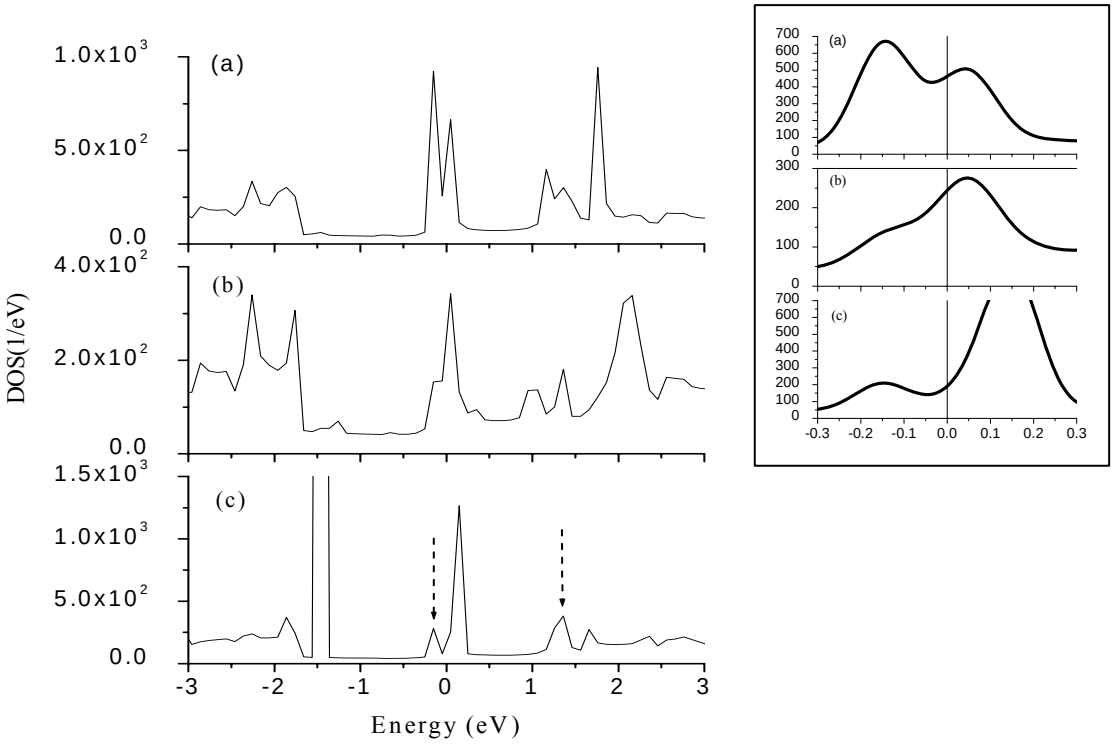

Figure 13 Plot of density of state of (a) Si_4O, (b) Si_4H, (c) Si_4 with Fermi level corrected energy. Inverted arrows for the bare Si cluster mark the fundamental HUMO-LUMO transition's spectral positions. Inset shows the zoom out DOS taken from the vicinity of Fermi energy that is also the zero point of the respective spectra. The straight line parallel to ordinate in the inset figure depicts the position of the zero point in the spectra.

In low dimensional systems like bare Si_n nano clusters, hydrogen and oxygen passivated Si_n nanoclusters, the charge transfer depends upon their quantum transport properties and the surface states. Among the spectra of bare, hydrogen and oxygen passivated Si_n nanoclusters there exist a steady DOS peak at the Fermi level which usually comes from the continuum states of graphene nanoribbon (ZGNR) of the left and the right electrodes. The DOS also explains how electrons are spectrally distributed in the nanodevice since the density of electrons or holes at the Fermi level directly determines the current transmission. From the DOS plot it is clear that we have significant density of states both around the spectral positions of fundamental transition as well as at the zero point. The former effect is easy to explain from the previously mentioned

electronic structure details but the later effect, which is responsible for the equilibrium or zero bias conductances, is purely a manifestation of a nano-electronic device phenomenon. Inset Figure 13(c) for bare Si_4 shows the value of ~100 for the equilibrium contributing states. Occurrence of such non semiconducting states in the previously eastalished semiconductor cluster can be explained with the help of various charge transfer process occurring in between the electrodes and Si_4 nanoclusters. The total charge transfer amounts to the value of 1.53548e, which also implies that significant LCR coupling is present in the device due to bond formations at the respective atomic contacts. A Figure 13(c) shows the DOS spectrum for bare nanoclusters and gives an idea about the origin of two resonant peaks that present around the Fermi level and spectrally positioned at -0.15 eV and 1.5 eV, which can be ascribed to the π related HOMO peak of the cluster and LCR coupling induced resonant peak respectively. But the peak indicated by arrow positioned at +1.2ev is certainly the spectral position of π* related LUMO state. It is worth to mention that for this system we have obtained the π- π* energy gap value of 1.25 eV in our electronic structure calculation given in the previous section. For this reason, such resonant peaks just above the Fermi level can only be attributed to the coupling induced effects.

However, by hydrogen or oxygen passivation of Si nanoclusters another variant of charge transfer concurrently takes place from nanocluster to passivant-atoms depending upon the electron affinities of the passivants in addition to the former process, which transfers the charge to the electrodes. This leads to another interesting observation in which the equilibrium conductance states increases in passivated structures of Si_4H and Si_4O up to the value ~250 and 500. Such respective double increment and five times enhancement from the value of zero bias states can only be explained with the help of the two mutually competitive processes of the charge transfer.

Distinguishably, a difference in the total charge on the electrodes and the central region along with passivant atoms gives an idea about the net amount of charge transfer taking place. Positive values of this difference indicates that the charge is transferred from the central region of the nano device to the electrodes. In the case of Si_4 the transferred charge values increases from 2.30634e to 2.63384e for Si_4H and Si_4O. Because in the case of oxygen passivation the more charge transfer is expected due to the strong electro negativity of the passivent. Hance charge transfer which increases from 14.46452e, 13.69366e and 13.3661e respectively among Si_4, Si_4H to Si_4O also shows increase in DOS at Fermi level. Dai et. al. have earlier reported the

similar studies on the effect of charge transfer from C_{60} molecule and Si4 cluster to Al electrodes [43, 45]. Therefore, based on the charge transfer we can say that the charge carrier scattering would be less in such passivated nanoclusters in comparison to the bare ones which would further facilitates the transport and improves the conduction across the nanodevices may be through several newly initiated resonant tunneling mechanisms. We found increased DOS at Fermi level due to these diverse charge transfer processes that takes place in the passivated structures of the Si_4 clusters.

We can also demarcate the π- π^* transition of the charge carriers in the DOS spectrum for Si_4H and Si_4O clusters with the help of as marked arrows in the DOS plot. In case of Si_4 the passivation is found to have little or no effect on the fundamental transition gap of the cluster when placed in the two probe device. This is a significant result from the device application point of view because in most of the previous studies authors have reported the variation in the electronic structure of nanomaterials on passivation. We attribute the origin of this effect to the enhanced stability of these very small nanoclusters. The observance of higher transition peaks in DOS spectrum are mainly ascribed to the high energy transitions like that of σ-σ^* excitations in nanoclusters or some other high energy resonant states that arise in the cluster due to the device related couplings. The increase in the contributing state with the increasing charge transfer from central region (CR) to electrode can be understood by the simple fact that less charge on CR will facilitate large electron tunneling from the CR due to less degree of electron-electron scattering.

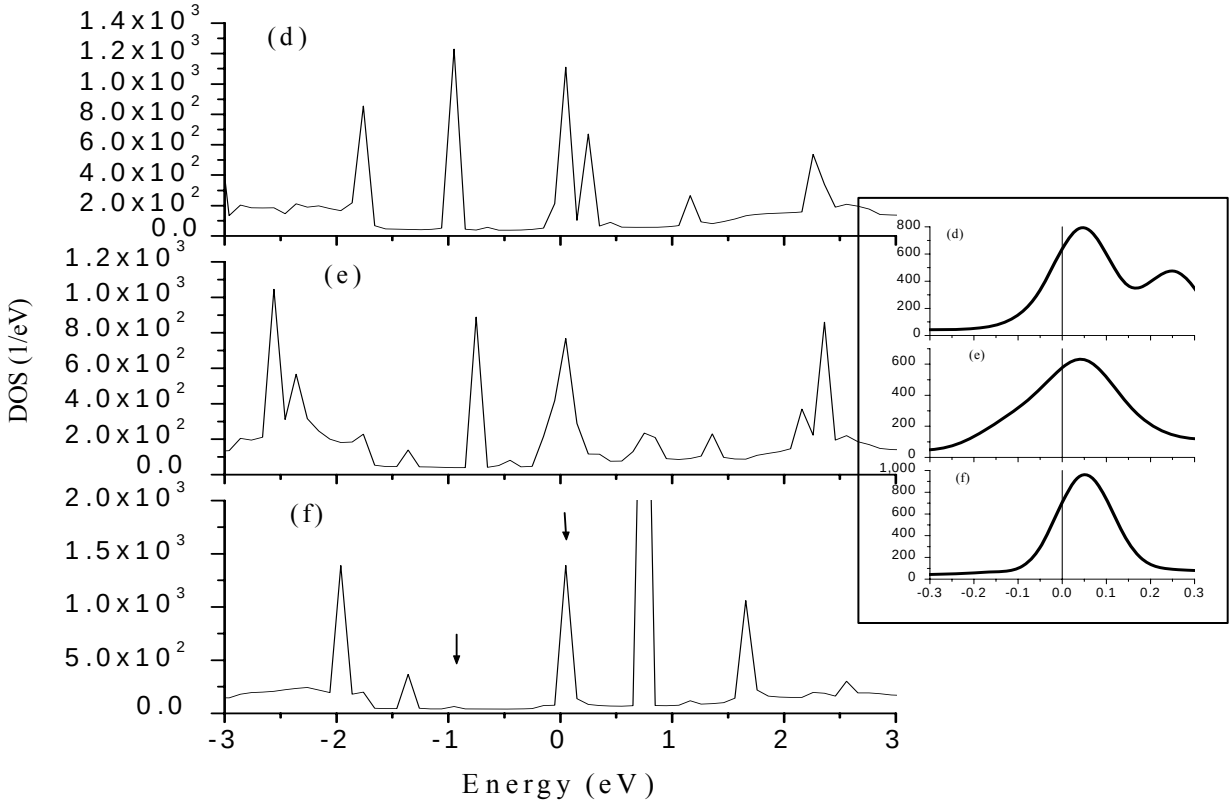

Figure 14 Plot of density of state of (d) Si_6O, (e) Si_6H, (f) Si_6 with Fermi level corrected energy. Inverted arrows for the bare Si cluster mark the fundamental HUMO-LUMO transition's spectral positions. Inset shows the zoom out DOS taken from the vicinity of Fermi energy that is also the zero point of the respective spectra. The straight line parallel to ordinate in the inset figure depicts the position of the zero point in the spectra.

For pure Si_6 nanoclusters the equilibrium contributing states have the value of around 800 in number. But on contrary the contributing state decreases with H and O passivation up to 600 for each of the passivated Si_6 cluster (see figure 14)as evident from the DOS spectra (inset). The π-π* transition is also obtained from the HOMO level positioned very close to the Fermi level and π* peak is situated at 0.65 eV (marked by the inverted arrow). In this structure, a slight change in the value of energy gap is observed which is within the limits of the error expectancy of DFT related calculations. To explain the rational of contrary observation of Fermi level state in Si_6H and Si_6O clusters we compare the charge transfer which takes place from cluster to the passivant atoms. We found the transfer values of 1.07392e from Si_4O to electrodes in comparison to that of 1.1360e for the present Si_6O. The increased electronic transfer in Si_6 could be due to the geometrical structure which is tetragonal bi pyramidal with higher stability as the total energy

per atom in the Si6cluster formation is -176.597 eV in comparison to Si_4 cluster which is -176.535 eV. Therefore, we anticipate that the higher stability of crystallographic structure of nanocluster allows more charge transfer to passivant atoms. Now more charge transfer to the oxygen or hydrogen atoms instead of the electrodes could lead to reduction in the coupling of the central region with the electrodes since the charge exchange in between them is an effective measure of their coupling strength. Finally, such reduced coupling lead to less flow of contributing states from the continuum electrodes to the discrete nanocluster, hence decrease in the DOS at the Fermi level.

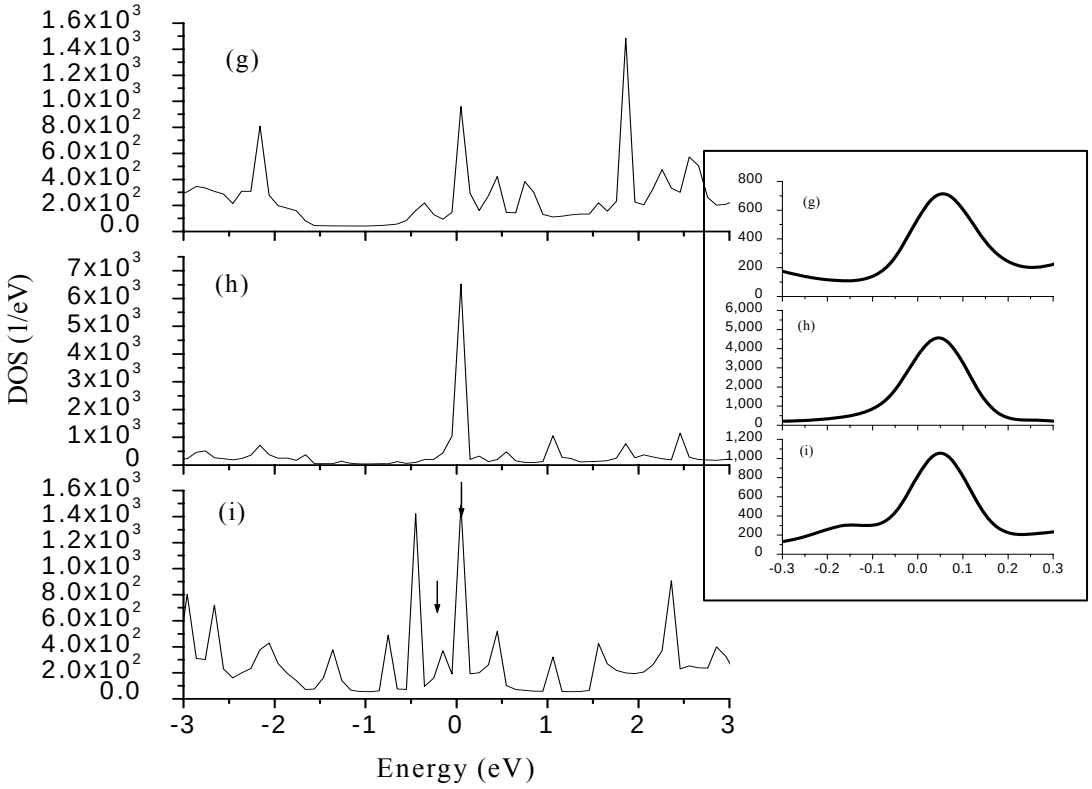

Figure15 Plot of density of state of (g) Si_7O, (h) Si_7H, (i) Si_7, with Fermi level corrected energy. Inverted arrows for the bare Si cluster mark the fundamental HUMO-LUMO transition's spectral positions. Inset shows the zoom out DOS taken from the vicinity of Fermi energy that is also the zero point of the respective spectra. The straight line parallel to ordinate in the inset figure depicts the position of the zero point in the spectra.

To concentrate on the very purpose of nanoswitching effect we limit our discussions to the zero bias density of states, which is found to be more important to explain the effect. Hence, in case of Si_7, the respective DOS values at Fermi level are as follows, 900, 4000 and 600 for the bare and passivated structures (see figure 15). As usual due to increased charge transfer, which is 3.6572e per atom for bare Si_7 to 3.6088e per atom for Si_7H and takes place from central region to electrode, we have obtained the increased value of equilibrium DOS of hydrogen passivated nanocluster. But in the case of Si_7O the charge transfer in fact decreases due to charge values of 3.6399e per atom, which is also manifested from decreased DOS value in Si_7O. We ascribe this change to the differently oriented oxygen atoms in the stable geometrical structure of Si_7O cluster. In fact, owing to this effect, the charge transfer to the different oxygen atoms is found to be very different varying from 6.3504e to 6.5563e per atom. Hence, the different types of adsorption by vivid orientations of O-atom to the surface of the nanocluster lead to the differential charge transfer to the passivents. Also the dimunitive values of charge transfer to O atom with respect to the H-atom implies that Si_7O passivation should give reduced values of DOS at the Fermi position. Similarly, in the DOS spectrum of Si_8 clusters that is given in the following figure 16 also track the parallel trends of earlier DOS results which leads to dependence of equilibrium conducting states on the charge transfer. However, in Si_8 we observe the decrease in charge transfer to the electrodes with respect to passivation. The average charge values per Si atom increases in these nanoclusters having the values of 3.69815e, 3.8264e and 3.6486e for Si_8, Si_8H and Si_8O respectively. As we know the decrease in charge per Si atom also corresponds to the increase in charge transfer from the central nanocluster to left and right electrodes. Therefore, the states at Fermi level in Si_8 system decrease from initial value of 2200 to 700 and 500 with H and O passivations.

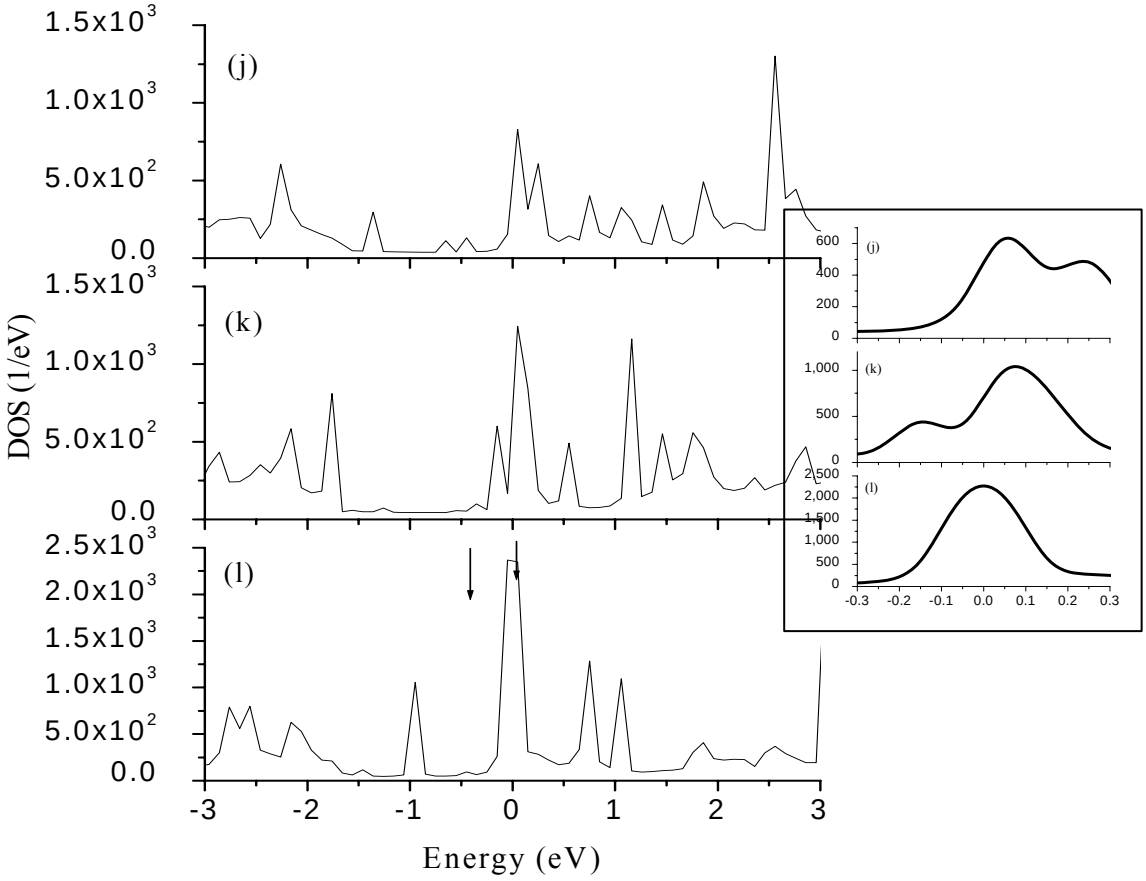

Figure 16 Plot of density of state of (j) Si_8O, (k) Si_8H, and (l) Si_8. With Fermi level corrected energy. Inverted arrows for the bare Si cluster mark the fundamental HUMO-LUMO transition's spectral positions. Inset shows the zoom out DOS taken from the vicinity of Fermi energy that is also the zero point of the respective spectra. The straight line parallel to ordinate in the inset figure depicts the position of the zero point in the spectra.

4.4 Transmission spectra of bare and passivated Si_n (n=4, 6, 7 and 8) clusters

The transmission spectrum of any device is typically used to inspect its charge transport behavior. Our two probe nanodevice is made up of a Si nanocluster sandwiched in between the two graphene ribbon electrodes. A figure 17 (a-l) shows the transmission spectrum of the ZGNR/Si_n/Si_nH/Si_nO/ZGNR two probe devices. The zero energy reference is taken at the Fermi level (E_f). The transmission peaks around the Fermi level is again found to appear in most of the T spectra of nanocluster devices.

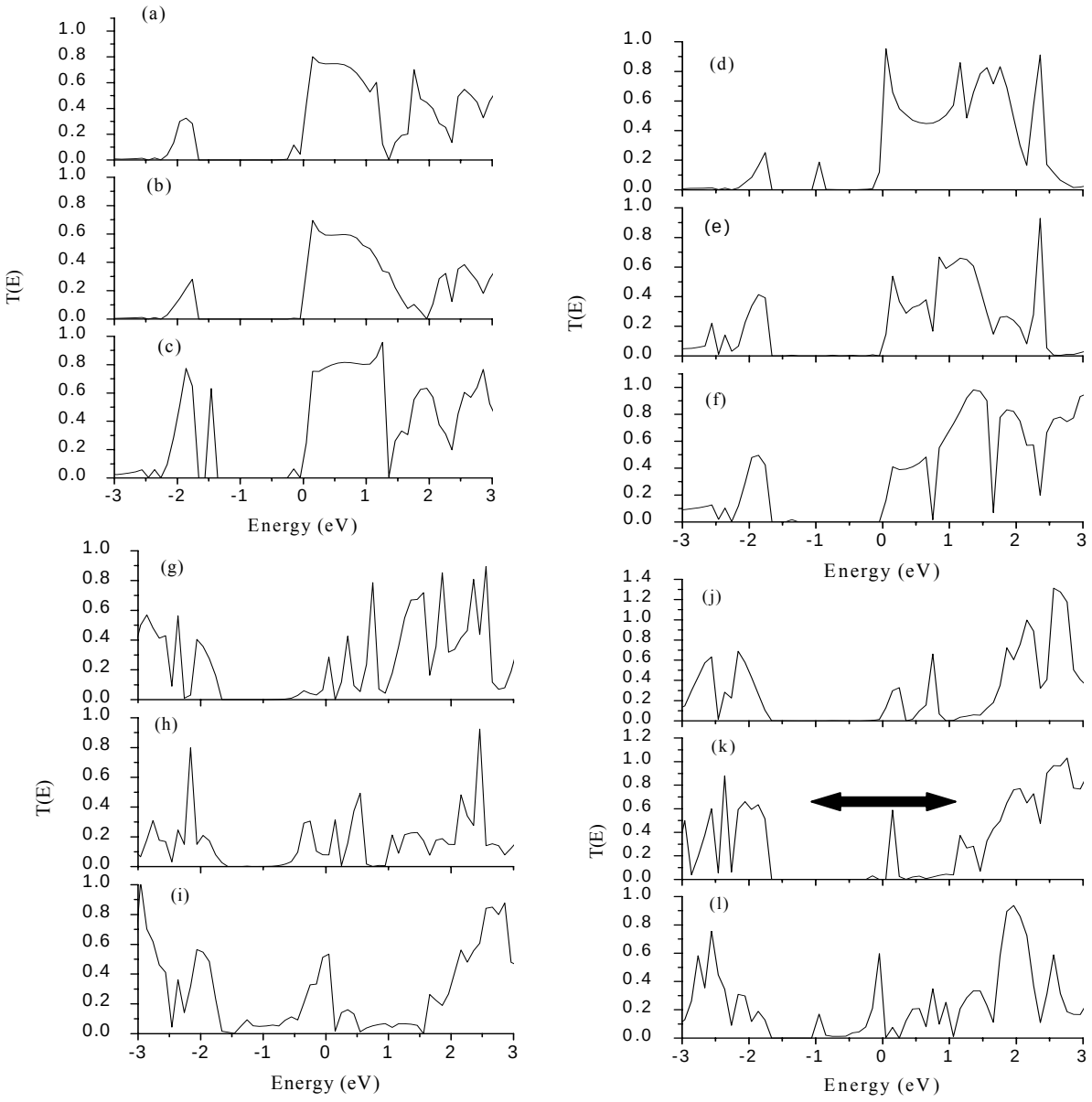

Figure 17 Transmission spectra of (a) Si_4O, (b) Si_4H, (c) Si_4, (d) Si_6O, (e) Si_6H, (f) Si_6, (g) Si_7O, (h) Si_7H, (i) Si_7, (j) Si_8O, (k) Si_8H, and (l) Si_8 nanoclusters are plotted as a function of Fermi corrected energy. The peak at the zero point represents the presence of metallic states in the cluster transferred from the bulk ribbon electrodes. The broad horizontal bar in the spectrum labeled 'k' shows the position of the transmission less plateau.

As we can obviously observe from the spectra given in figure 17 that most of the electron transmission characteristics occur in the respective nano-devices follow the broad trends of the previously studied respective DOS spectra. Also we know from the previous sections that in most of our passivated and unpassivated Si_n nanoclusters device, the dispensing of the equilibrium conducting states from the electrode to the nano-cluster regions is observed. Hence, it's an exceedingly adverse for nanoswitching that instead of having well illustrated semiconductor like characteristics, these nanoclusters inside the two probe device are not much practical for device deployment due to the absence of desired rectification and the ON/OFF ratio with minimal leakage current requirements. This is also corroborated from as shown transmission results in which the equilibrium states give rise to the transmission of very low energy electrons at the zero bias. As per se the known criterion followed in the nanoswitching processes, the Fermi level charge transmission should be as low as possible for attaining effective ON/OFF ratios. Nonetheless, if look carefully at the T(E) spcetras of Si_8 clusters, we can easily figure out that in the H passivated spectrum there is a presence of large plateau around the Fermi level which is almost transmission less, and accompanied bywith an exception of small peak around the upper end of zero position. The extent of this plateau in the figure is also marked by a bold horizontal arrow indicator. The plateau width is found to be ~2.7 eV, which in itself is a very large value, which enables the ON passage only for higher energy electrons i.e. up to the external bias value of ~3 V. This is an exceptional result because most of the nanoswitches in present the quantum dot technology operate only at low voltages, hence fore they can never be able to get deployed for more practical power electronics applications. Of course, this is mainly owing to the low values of their T-less plateaus. Hence we can say that the Si_8H nanocluster is a superior nano switch, especially for high frequency and high voltage operations. However due the presence of a small upper end peak at ~0.3 eV, we can also anticipate that this switch would show some leakage current during the switching process. Nevertheless, the leakage would remain negligible for high energy charge carriers because this small T(E) peak decreases exponentially with energy as discernible from the concern spectrum.

4.5 Nonequilibrium Dynamics

4.5.1 I-V measurements on bare and passivated Si_n (n=4, 6, 7 and 8) nanoclusters

The current-voltage (I-V) calculations are preformed using the Nonequilibrium Green's function formalism combined with the density functional theory (NEGF/DFT). A figure 14(a-d) shows the calculated I-V curves for Si_n, Si_nH and Si_nO junction by NEGF/DFT method. We can depict from the I-V curve that the nanoclusters of Si_n, Si_nH and Si_nO in contact with ZGNR exhibit rise and fall of the current with the movement of the transmission peaks since the charge carrier transmission probability dominates the magnitude of the current owing to the vicinity of T-resonance peak to the Fermi level. In two probe devices of bare, hydrogen and oxygen passivated Si_4, Si_6 and Si_8 clusters, it is found that with a positive bias application an upshift of the transmission peak takes place that it is away from the Fermi level that results in a smaller electrical current. While the use of a negative bias shifts the transmission peak toward the Fermi level and leads to a bigger current. Therefore, the current is smaller for the positive bias than that for the negative one (see figure 14 (a, b and d)). The two probe device of ZGNR/Si_7/Si_7H/Si_7O/ZGNR applied a positive bias and due to an upshift of the transmission peaks which makes them closer to the Fermi level and hence results in a higher electrical current, while a negative bias shifts the transmission peak far away from the Fermi level and leads to a lesser electrical current. An admirable switching properties are obtained for the devices which comprise of bare-Si_4, oxygen passivation of Si_7 and hydrogen passivation of Si_8 because of sudden rise of current in their I-V curves beyond 0.70 V, -1.0 V and 0.8 V respectively with the corresponding current ON/OFF ratio values of ~3.5, ~1.7 and ~29.5. The phenomenon of negative differential resistance is also apparent from the I-V curves of most of the samples especially it is more prominent in case of the bare nanoclusters of Si_4, Si_7 and Si_8. Signatures of NDR in various current voltage characteristics is well depicts from the decrease of the current on increasing the voltages towards positive bias. This is because of the fact that nanostructures are the few electron states systems, which give rise to singularities in the electron transmission channels. Especially we have observed such singularities in the π^* related LUMO transmission channel of the bare clusters which lead to sharp effects of NDR after the LUMO energy cross-

overs at bias voltages greater than >1.0 as illustrated from the I-V characterstics. This is one of the manifestations quantum confinements among these silicon nanoclusters.

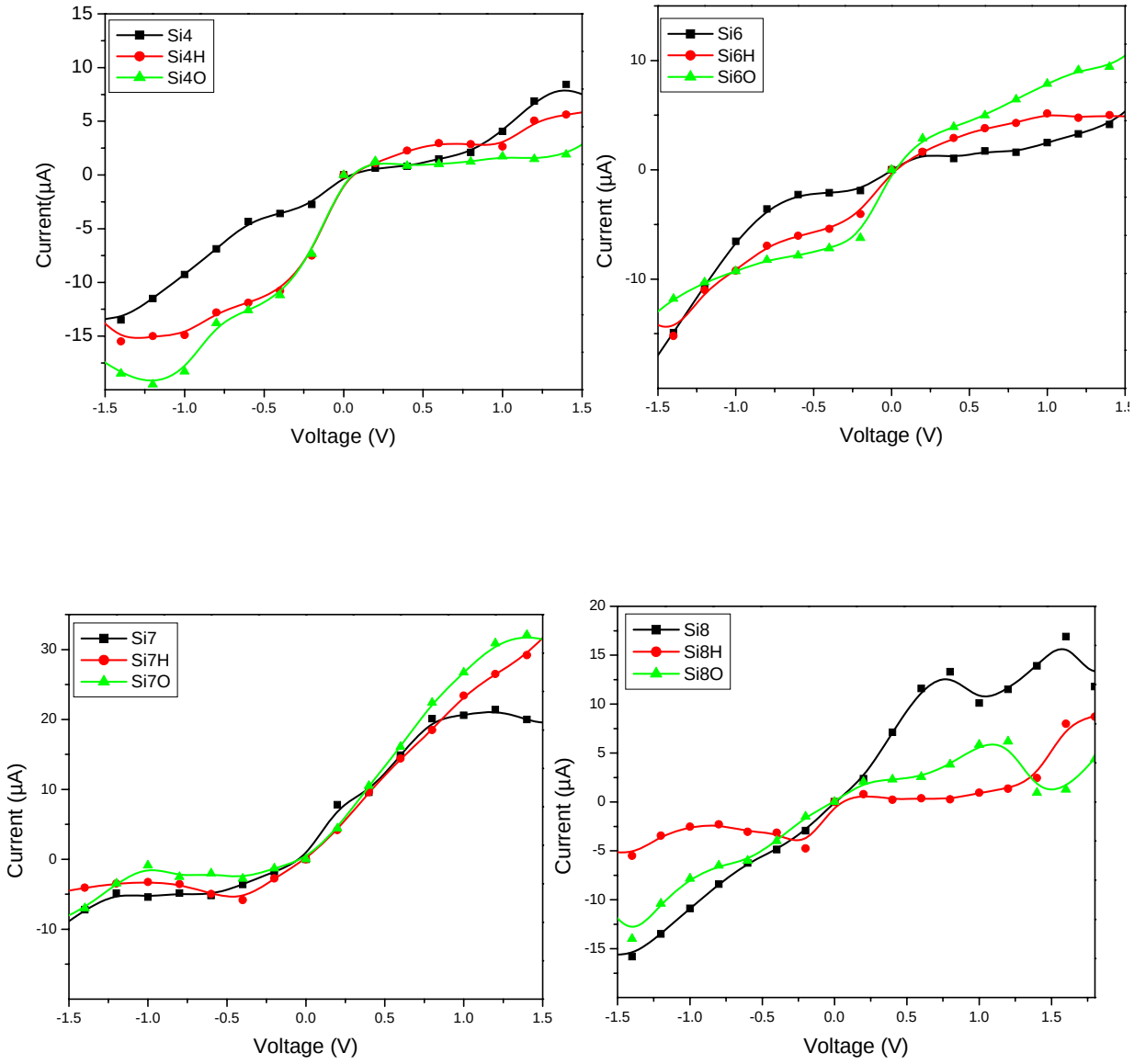

Figure 18 The current-voltage curves of the bare, hydrogen and oxygen passivation of (a) Si_4, (b) Si_6, (c) Si_7 and (d) Si_8 nanoclusters.

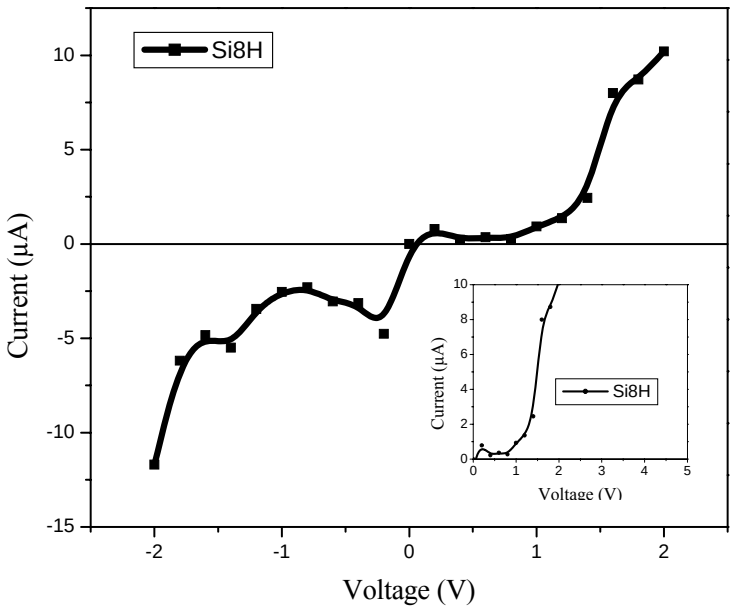

Figure 19 I-V characteristics of hydrogen passivation of Si_8H in the wider voltage range. Inset shows switching behavior of the nanocluster device in the operational voltage range.

As discussed previously in the transmission spectra results of Si_8H sample, the existence of a noteworthy transmission less plateau under the positive bias can be used effectively for the very purpose of nanoswitching. The as plotted I-V curve for this sample also shows the OFF state of the device for the bias range of -1.3 V to 1.5 V. The OFF state voltage range is as expectedly around 3V which matches very well with the width of the T-less plateau. After this range there is a sudden increase in the current that is apparent in the I–V curves and it can be defined as the ON state of the device. However the currents get saturated as the bias increased further. The sudden increase and saturation of the current arises either due to the available transmission channels as discussed before or due to singular LUMO associated contributing states of the cluster. Hence, the particular device also shows excellent switching with OFF state from 0-1.2 V and ON state for voltages >1.2 V. Thus there is a perfect switching from a non-conducting state (OFF) to a conducting state (ON) with the current ON/OFF ratio value of ~29.5 in this switching device.

Chapter Five

Conclusion

We have presented our detailed results for the ground-state structures and electronic properties of Sin, SinH and SinO clusters using LDA-DFT simulations. From our studies a high degree of structural stability is observed in very small Sin nanoclusters of various sizes ; n = 4, 6, 7 and 8. The energy gap in between LUMO-HOMO of the cluster decreases with "n" in accordance with general principles of quantum confinement from the initial values of 1.25 eV and down to 0.43 eV. However, the Si_6 nanocluster, due to its newly discovered super stability and from the present set of studies performed in this work, is found possess least average energy per Si atom and shows maximum stability conformation with gap energy of 0.45 eV which is surprisingly ~0.2 eV lower than the energy of its nearest neighbor. All the energy gap are calculated on the highly optimized geometrical structures with very low force tolerance values. We have also found that the cluster stability increases with passivation and the significant contributing states at the equilibrium energies are observed in the nano-devices made up of these nanoclusters, in which the clusters are positioned in the central region. The enhanced states at zero bias are extensively explained with the help of charge transfer effects, occurring in between the central region and electrodes as well as the passivant atoms. The extent of coupling in between various nano devices components, is found to be increasing with the amount of charge transfer to the electrode. This effect is endorsed to be responsible for the contributing state transfer from the electrodes to the central region as well as for an increase in equilibrium conductance due to a diminished electron-electron (e-e) scattering and the as emergent resonant tunneling states. An electron transmission across the central region of the nano device is mostly found to follow the trends that are established during our DOS studies. We have the significant equilibrium states in some of the nano device which is credited to the large extent of coupling of clusters with the attached electrode. However, we also found some of the nano devices useful for their deployment in the nanoswitching due to the presence of broad transmission less plateus near Fermi level in their T(E) spectrum.

Finally, we have also determined the current-voltage characteristics (I-V) of ZGNR/Sin/ZGNR of bare and passivated of Sin nanoclusters. The I-V characteristics curve of

the ZGNR/Sin/ZGNR shows strongly nonlinearities along with negative differential resistances as a result it can be used for a nano-switch. The origin of NDR effects in nanodevices is ascribed to the presence of quantum confinement induced singularities among various nanoclusters. Conclusively, we have found that the Si8H nanocluster two probe device posseses is excellent switching properties as compare of the others with higher ON/OFF ratio ~29.5.

References

1. Shvartsburg AA, Liu B, Jarrold MF, and Ho KM (2000) J. Chem. Phys., **112**: 4517-4523.
2. Pawlak B J , Gregorkiewicz T, Ammerlaan J (1998) Phys. Stat. Sol., **210**: 631-634.
3. Pan J and Ramakrishna MV (1994) Phys. Rev. B **50**, 15431-15434.
4. Dai Z X, Zheng XH, Shi XQ, and Zeng Z (2005) Phys. Rev. B **72**: 205408-205412.
5. Bergeron DE and Castleman AW (2002) J. Chem. Phy., **117**: 3219- 3223.
6. Nishida M. (2005) J. Appl. Phys., **98**: 023705- 023710.
7. Liz-Marzán LM, and Kamat PV. (2004) Nanoscale materials, Kluwer, New York, pp.1-5
8. Xiaolei Z, Xiao CZ (2003) J. Chem. Phys., **118**: 3558-3570.
9. Aronstein D L and Stroud C R. (1997) Phys. Rev. A **55**: 4526- 4537.
10. Hawrylak P. (1999) Phys. Rev. B **60**: 5597- 5608.
11. Bart Van Zeghbroeck *(2011)* Principles of Semiconductor Devices, *Colarado University, Colarado, pp. 57-69.*
12. Chang QS, Tay BK, Li S, Sun XW, Lau SP and Chen TP (2001) Mater. Phys. Mech., **4**: 129-134.
13. Pan LK, Chang QS, Chen TP, Li S, Li CM and Tay BK (2004) Nanotechnology **15**:1802–1806.
14. Shinji N, (2010)**,** Device Applications of Silicon-Related Nanoparticles. URL: http:// nano.ee.uec.ac.jp
15. Rene F, Susan BS, and Andrew ED (1992) J. Chern. Phys., **97**:4149- 4161.
16. Bao-xing L, Pei-lin C, and Xu-yan Z (2003) Phys. Stat. Sol. (b), **238**: 11-19.
17. Nalwa HS. (2002) Handbook of Thin films Materials: Nanomaterials and Magnetic Thin Films, Vol 5, Academic Press**,** Waltham Massachusetts, pp. 20-55
18. Pavesi L, Bettotti P, Cazzanelli M, Dal Negro L, Danese B, Gaburro Z, Oton CJ, Prakash V and Pavesi L (2002) *J. Phys. Condens. Matter, **14**:* 8253- 8281.
19. Ghoshal SK, Jain KP and Elliott RJ (2005) J. Metastable and Nanocrystalline materials, **23**: 129-132.
20. Tatsuro M, Eiichi S, Isao S, Mitsuyuki Y and Kenichi I (1999) *Nanotechnology, **10**:* 127-131.
21. Aaron P, Williamson AJ, Jeffrey CG, and Giulia G (2002) Phys. Rev. Lett. **88**: 097401-097406.

22. Vector EB. (2007) A handbook on Nanoscience and Nanotechnology, Wiley-VCH Velarg Gmbh & Co.KGaA, Weinheim, pp. 135-215.
23. David QA, Gemma CS, Richard PV, and Mark AR (2008) J. AM. Chem. Soc., **130**: 17309-17319.
24. Benjamin G. (2010). Hydrogen Passivation of Polycrystalline Si Thin Film Solar Cells. PhD thesis, Berlin University, pp 20-35.
25. Menghao W, Xiaojun W, and Xiao CZ (2010) J. Phys. Chem. C**, 114**, 3937–3944.
26. Yi-Peng A, Chuan-Lu Y, Mei-Shan W, Xiao-Guang M, and De-Hua W (2009) J. Chem. Phys. **131**: 024311-024317.
27. Andrey EM (2010) Rev. Mod. Phys., **82**: 2257- 2298.
28. Liu S, Liu X, Li Z, Yang S and Wang J (2011) New J. Chem. **35**: 369–374.
29. Hyunwoo K, Ahmed AA, and Christopher WM (2010) Macromolecules, **43**(16): *6515*-6530.
30. Fano U. (1961) Phys. Rev. **124**: *1866–1878*.
31. Xingqiang S, Zhenxiang D, and Zhi Z (2007) Phys. Rev. B **76**: 23541.
32. Dai ZX, Shi XQ, Zheng XH, Wang XL and Zeng Z (2007) Phy. Rev. B **75**: 155402-155410.
33. Dai ZX, Shi XQ, Zheng XH, and Zeng Z (2006) Phys. Rev. B **73**: 045411-045415.
34. Xiaohong Z, Zhenxiang D and Zhi Z (2009) J. Phys. Condens. Matter, **21**: 145502-145505.
35. Jeremy T, Hong G, and Jian W (2001) Phys. Rev. B **63**, 121104-121104.
36. Sherrill CD (2005) The Born-Oppenheimer Approximation, Georgia Institute of Technology, Georgia, pp. 20-150.
37. Wolfram K, Max CH (2001) A Chemist's Guide to Density Functional Theory, Wiley-VCH, New York, pp. 50-200.
38. Taisuke O, Kengo N, Hiori K (2010) Phys. Rev. B **81**: 035116-035147.
39. Bernhard Schlegel H (2011) Adv. Rev. **00**: 1-12.
40. http://www.hpcx.ac.uk/research/chemistry/siesta.html
41. Atomistix Toolkit(Tutorial and Reference Guide), Version 2.0 www.quantumwise.com/manuals/ATK_2.0.4_Tutorial_and_Refere.
42. Virtual NanoLab (Tutorial), Version 2008.10

www.quantumwise.com/documents/manuals/vnl-2008.10-tutorial

43. Sashidhar G, Ghaisas SV, Sundararajan V (2008) Sol. Sta. Phen., **139**: 113-118.
44. Dai ZX, Zheng X H, Shi XQ, and Zeng Z (2005) Phys. Rev. B **72** : 205408-205417.
45. Yi-Peng A, Chuan-Lu Y, Mei-Shan W, Xiao-Guang M, and De-Hua W. (2009) J. Chem. Phys., **131**: 024311-024317.